Contents

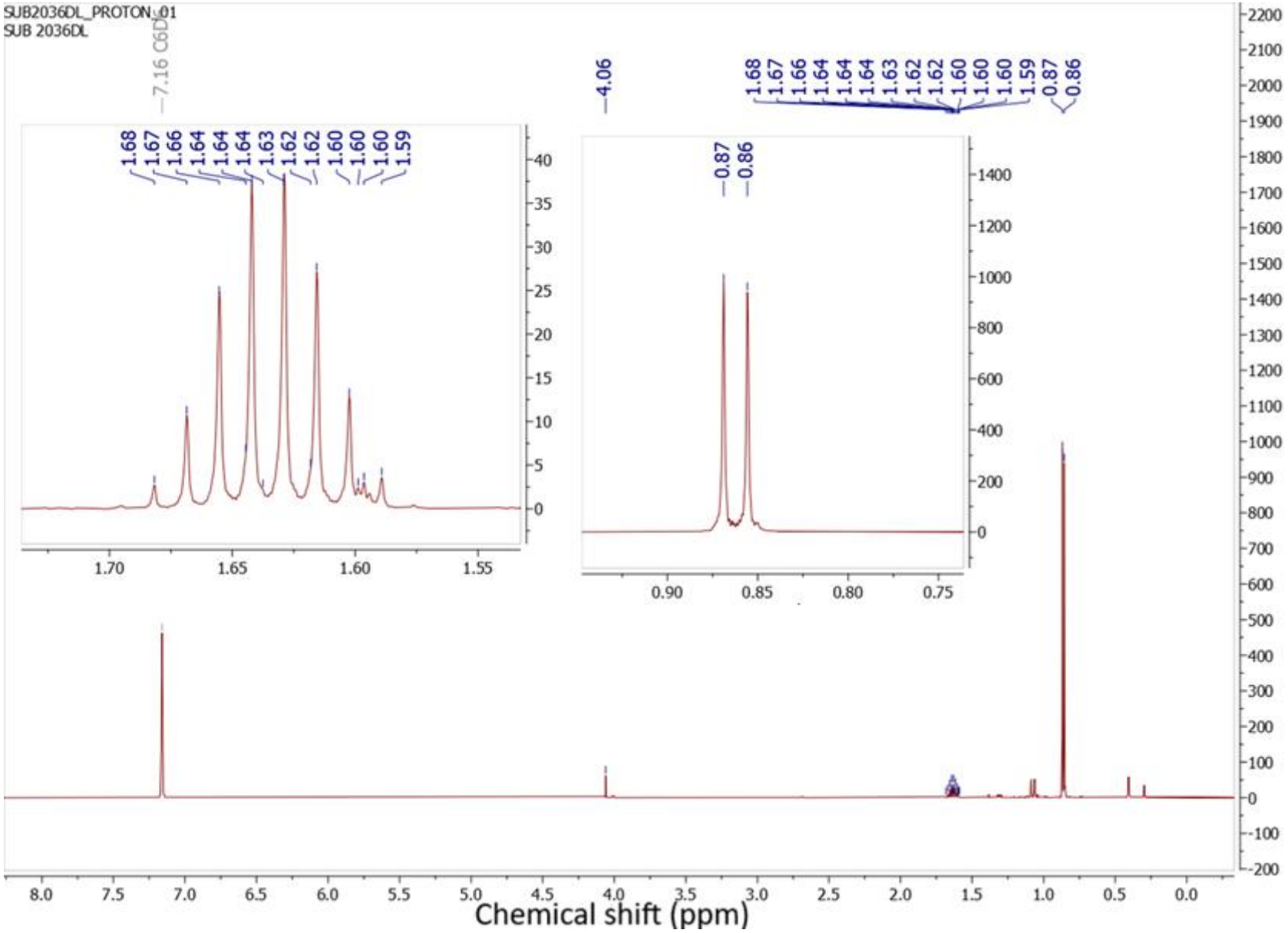

Fig S1. ^{1}H NMR spectrum of soluble fraction from the polymerization of **1**.

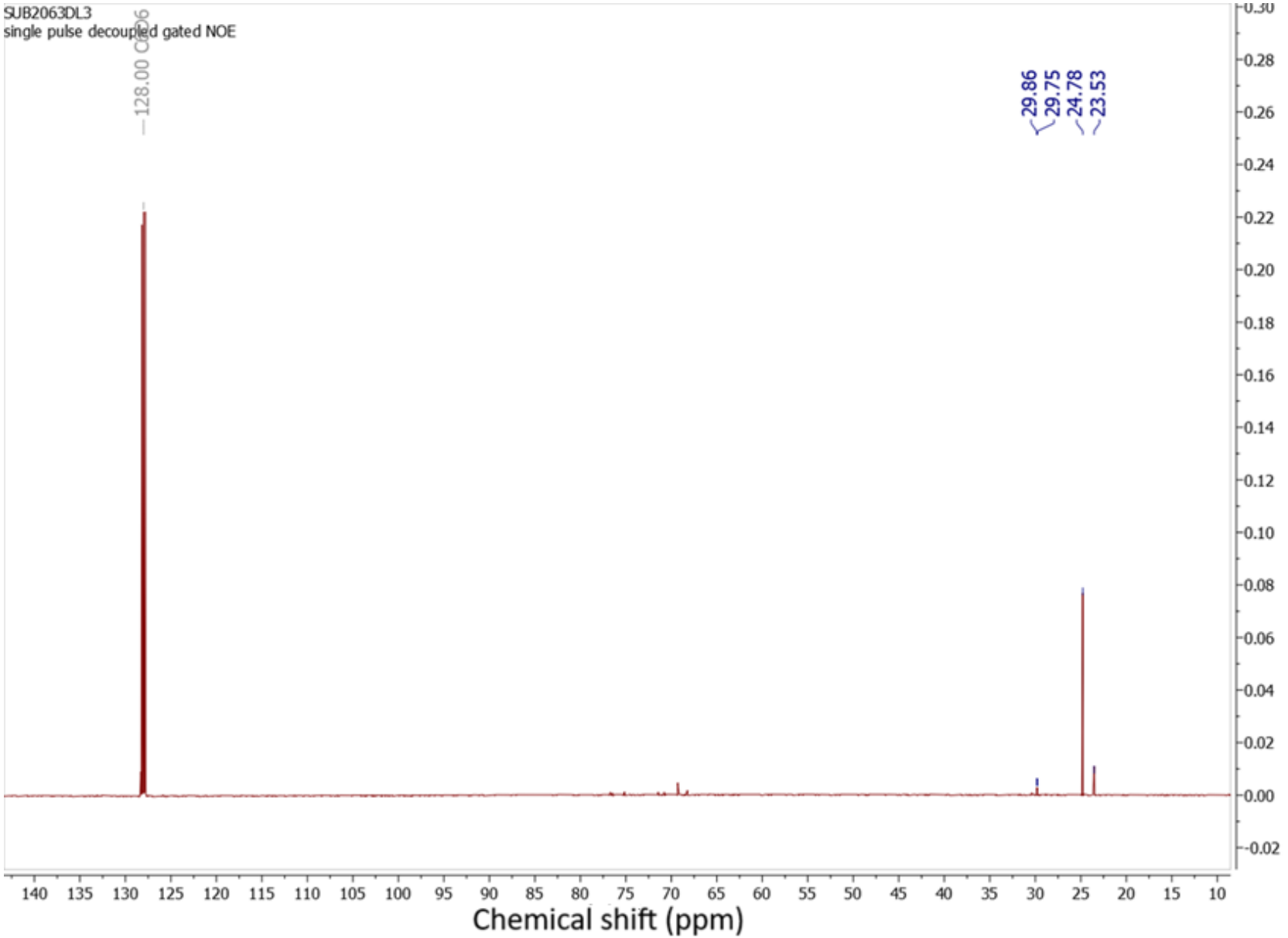

Fig S2. ^{13}C NMR spectrum of soluble fraction from the polymerization of **1**.

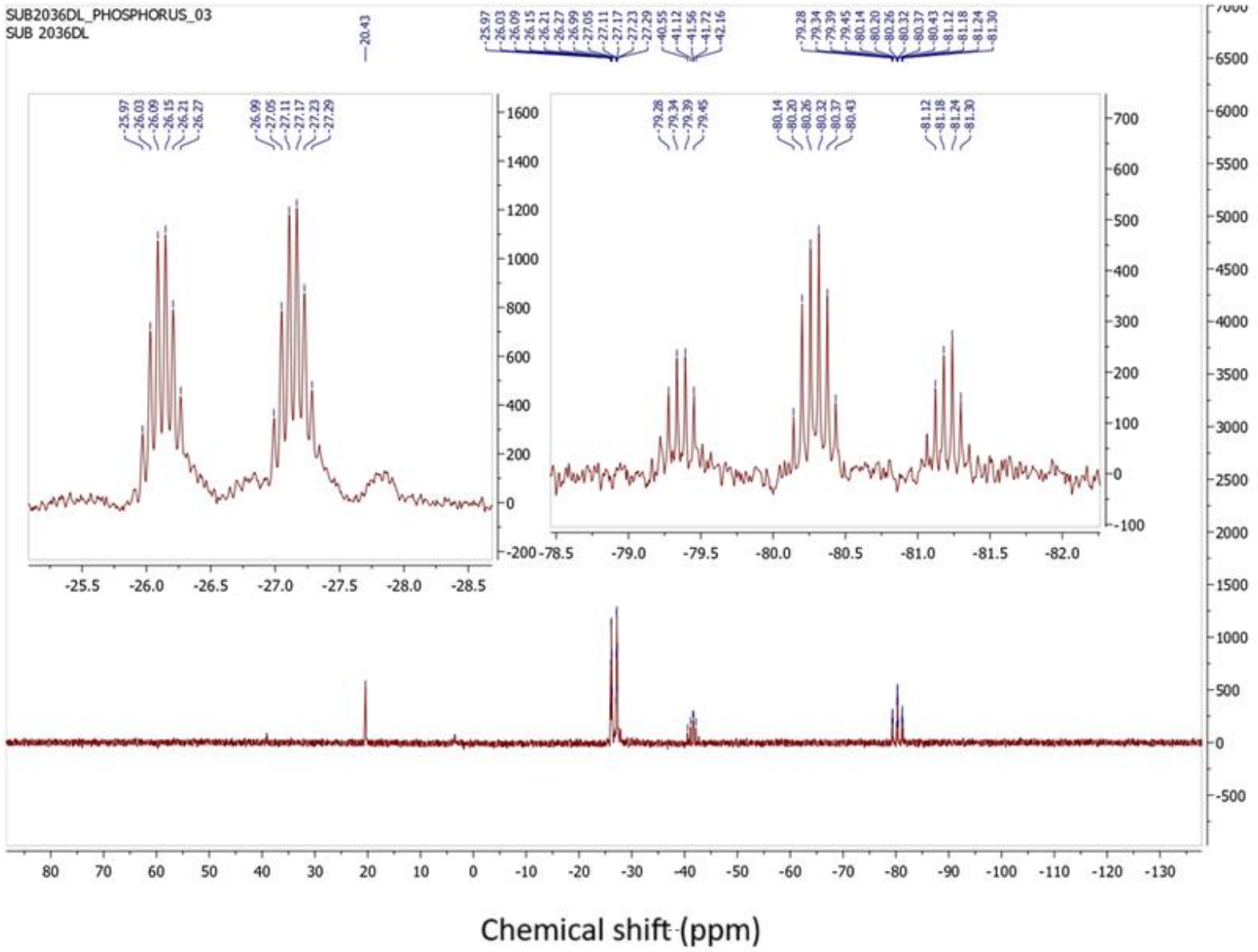

Fig S3. ^{31}P NMR spectrum of soluble fraction from the polymerization of **1**.

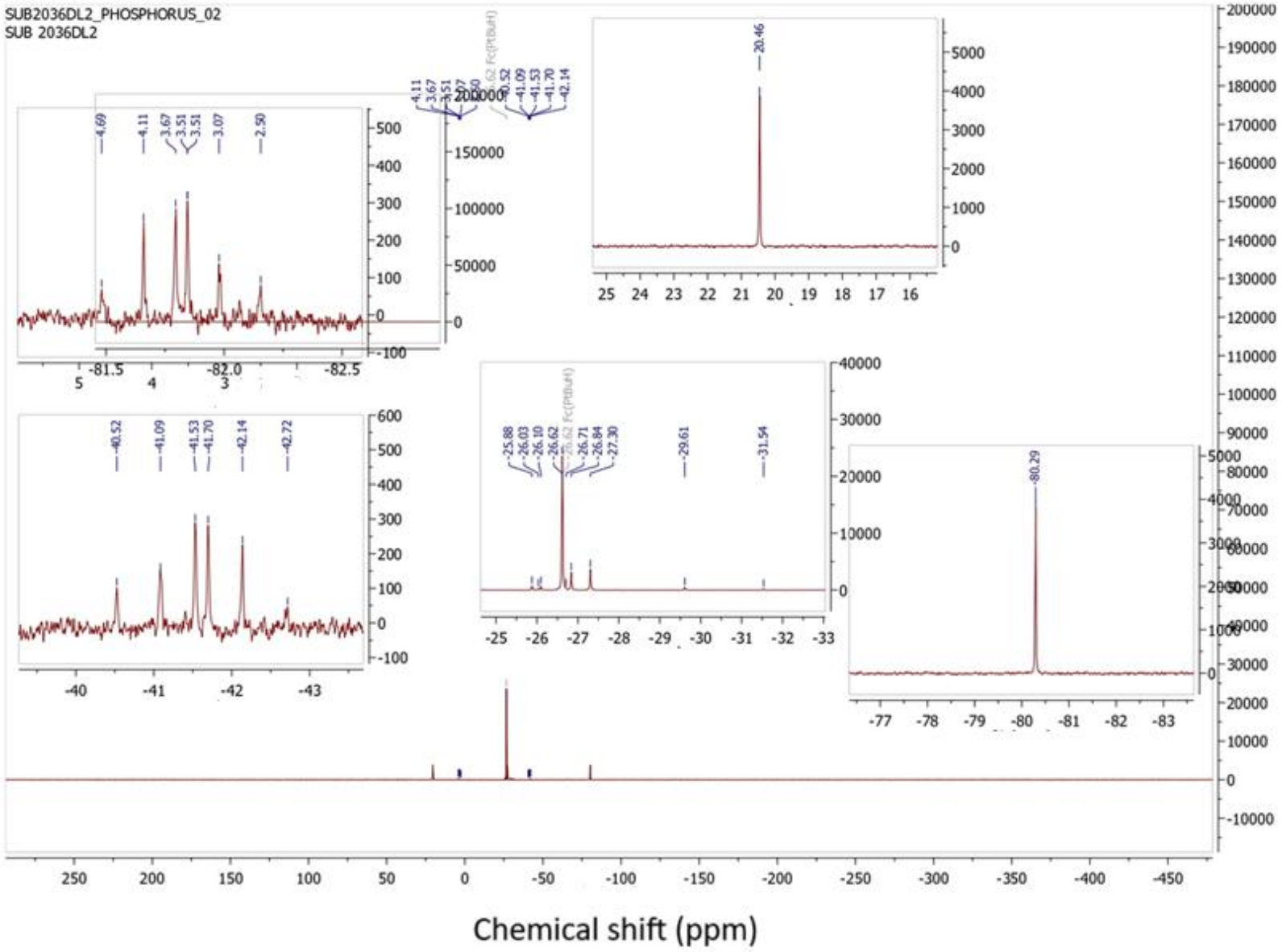

Fig S4. ^{31}P {^{1}H} NMR spectrum of soluble fraction from the polymerization of **1**.

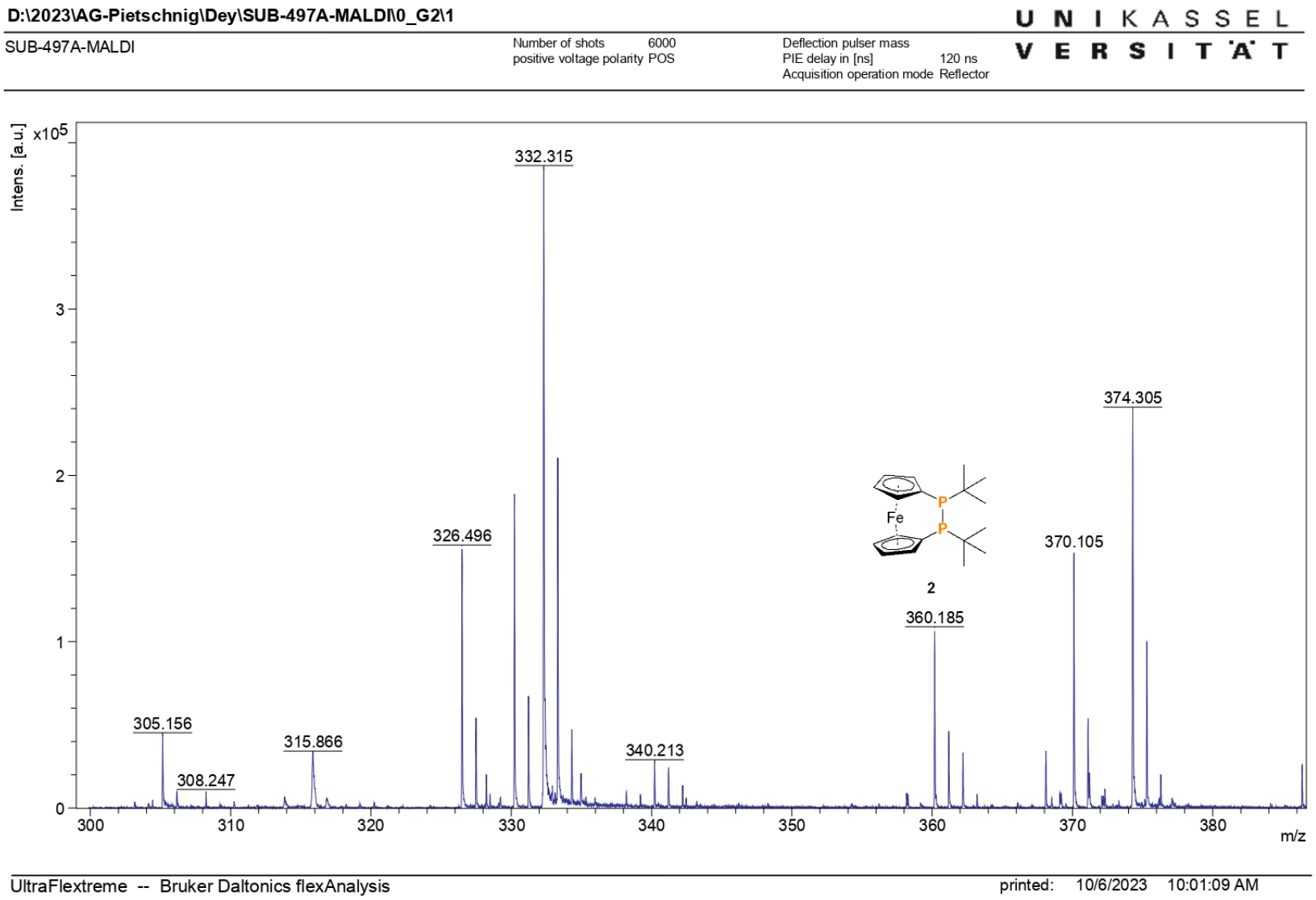

Fig S5. MALDI spectrometric analysis from soluble fraction from the polymerization of **1**, showing corresponding peaks for **2**.

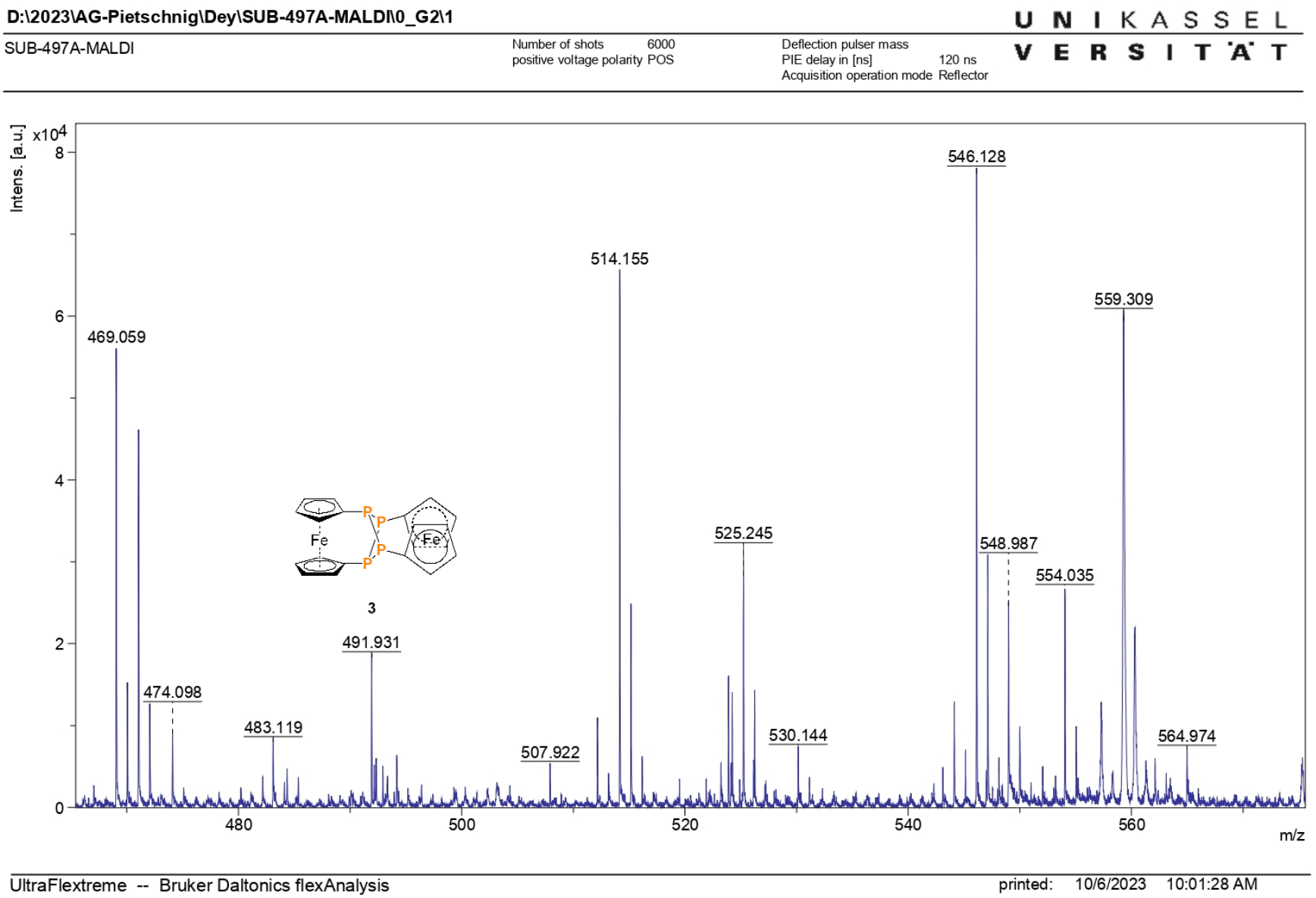

Fig S6. MALDI spectrometric analysis from soluble fraction from the polymerization of **1**, showing corresponding peaks for **3**.

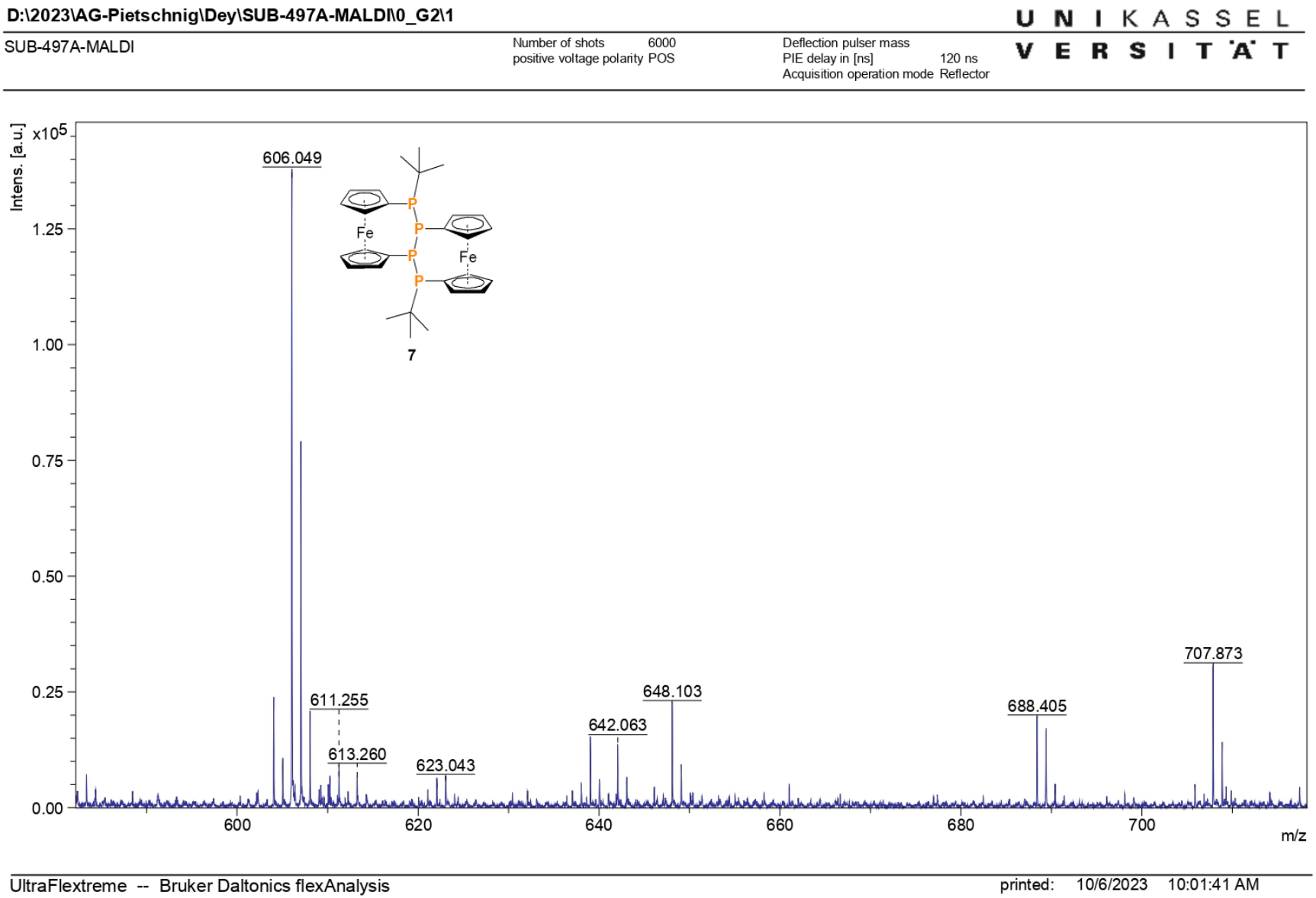

Fig S7. MALDI spectrometric analysis from soluble fraction from the polymerization of **1**, showing corresponding peaks for **7**.

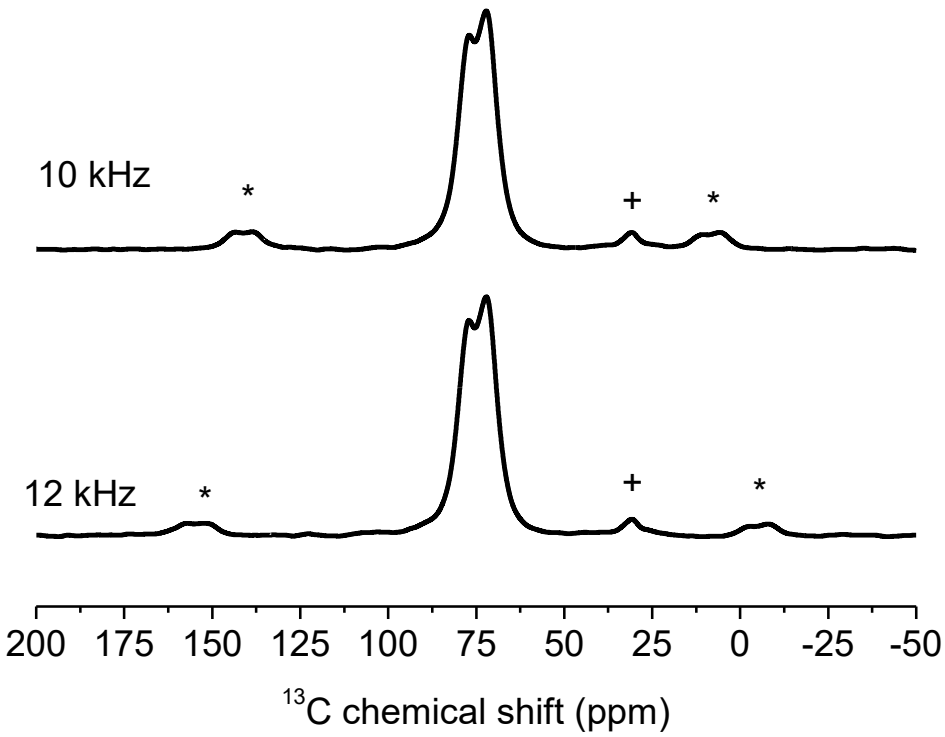

Fig S8. Comparable perspective of ^{13}C CP MAS NMR spectra of polymer **5**, measured at 14 T at 10 and 12 kHz spinning, respectively.
Note: Spinning sidebands are marked with asterisks and plus.

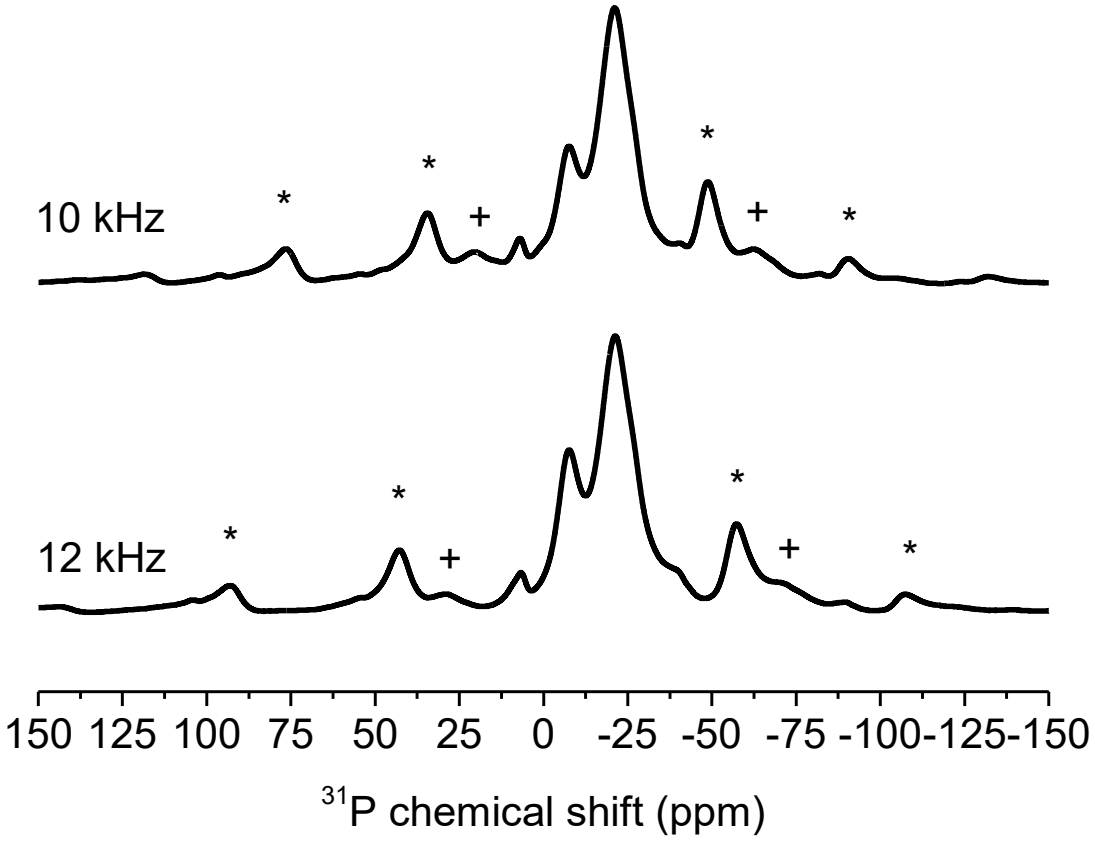

Fig S9. Comparable perspective of ^{31}P CP MAS NMR spectra of polymer **5**, measured at 14 T at 10 and 12 kHz spinning, respectively.
Note: Spinning sidebands are marked with asterisks, plus, minus and tilde.

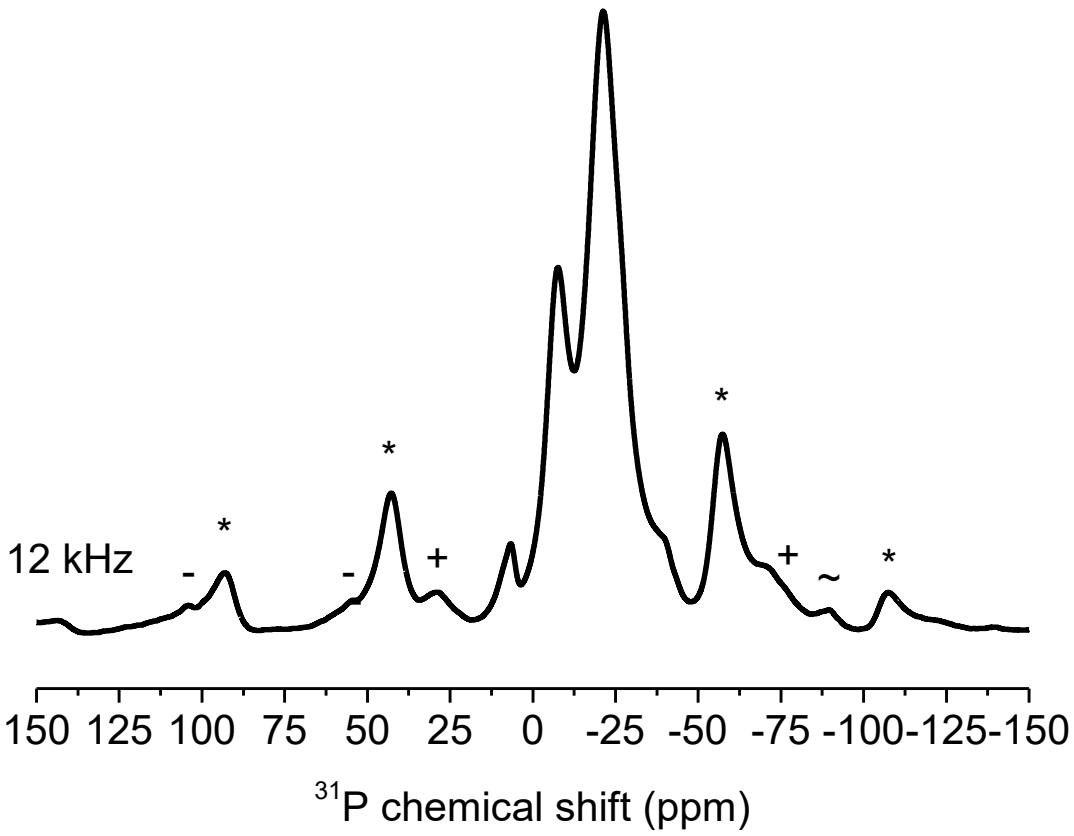

Fig S10. ^{31}P CP MAS NMR spectra of polymer **5**, measured 14 T at 12 kHz spinning.
Note: Spinning sidebands are marked with asterisks, plus, minus and tilde.

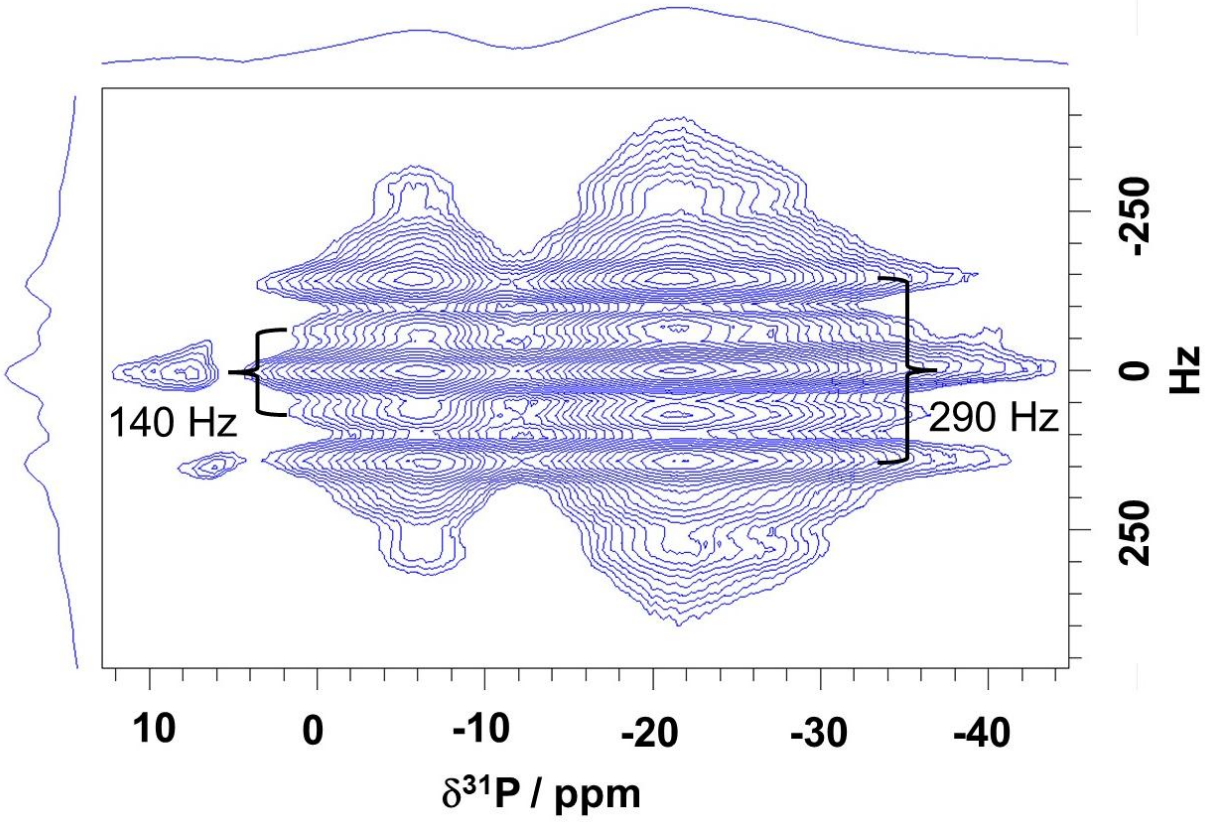

Fig S11. ^{31}P *J*-resolved NMR spectrum of polymer **5**, measured at 12 kHz spinning.

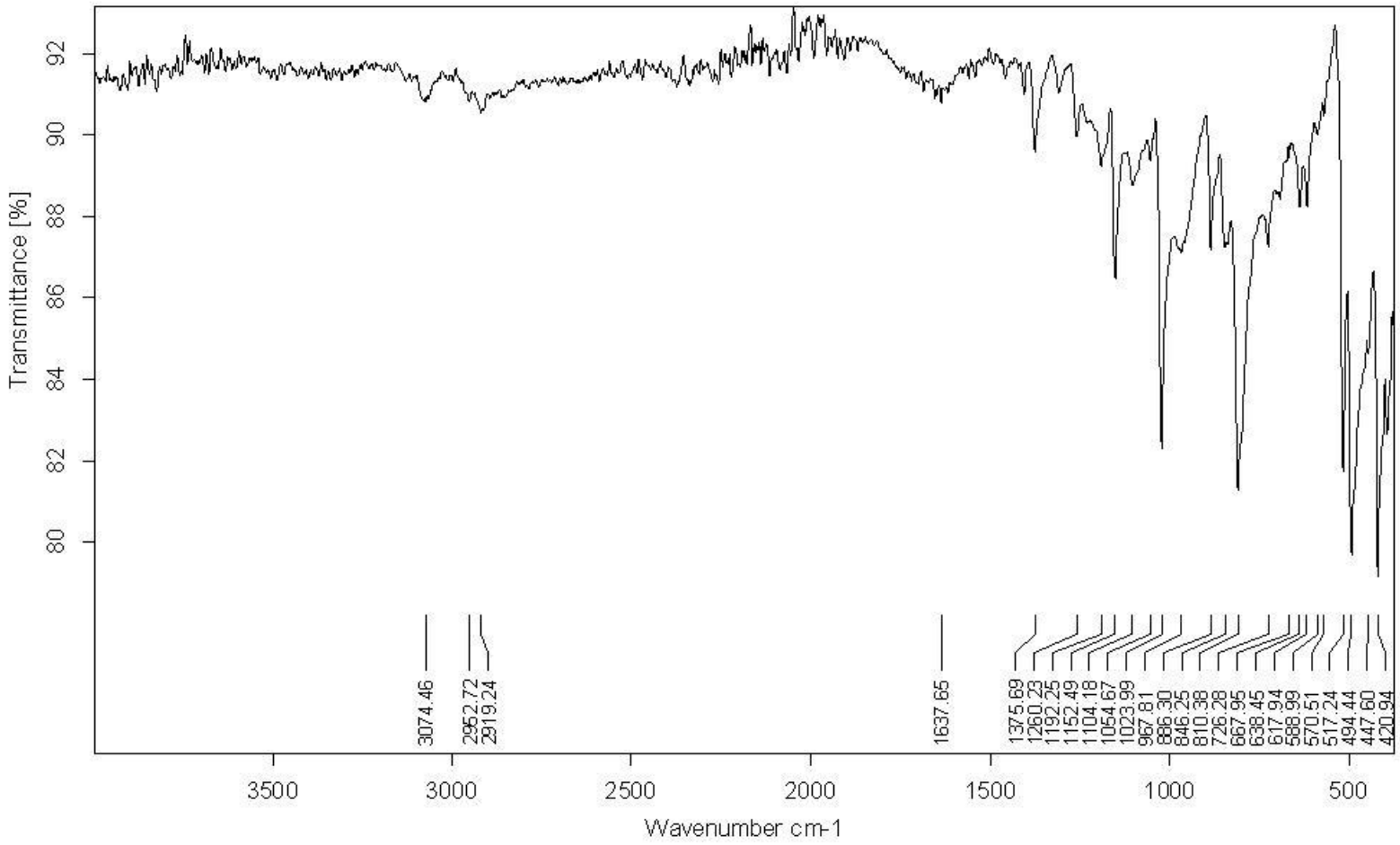

C:\Programme\OPUS_65\MEAS\SUB560.0	SUB560	Instrument type and / or accessory	27/01/2023
C:\Dokumente und Einstellungen\Admin\Desktop\IR\AG Pietschnig\Subhayan\SUB560.0	SUB560	Instrument type and / or accessory	27/01/2023

Seite 1 von 1

Fig S12. Solid state ATR-IR spectrum of polymer **5**.
The full characterization of **5** is reported in article reported by Pietschnig *et. al*.[1]

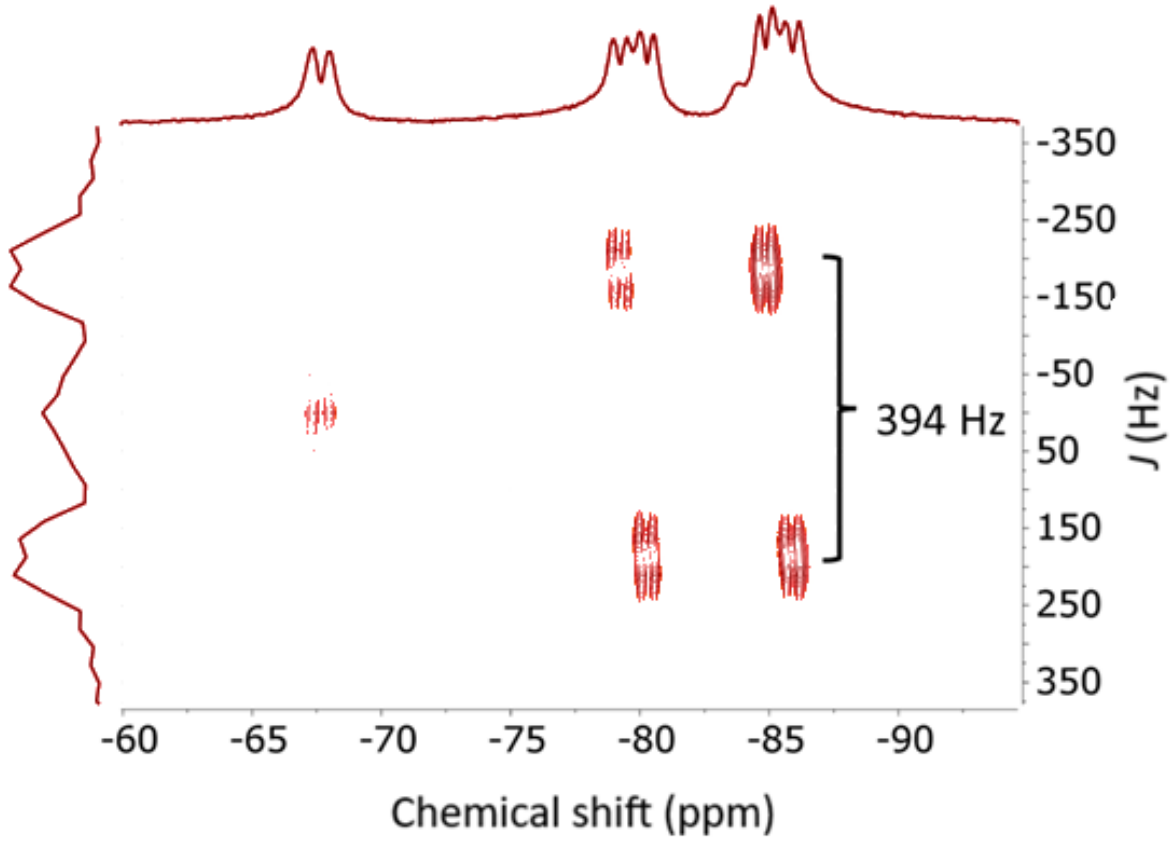

Fig S13. ^{31}P *J*-resolved NMR spectrum of Wilkinsons-Catalyst, measured at 12 kHz spinning.
Note: $^{2}J(^{31}P\text{-}^{31}P)_{trans}$ = 394 Hz

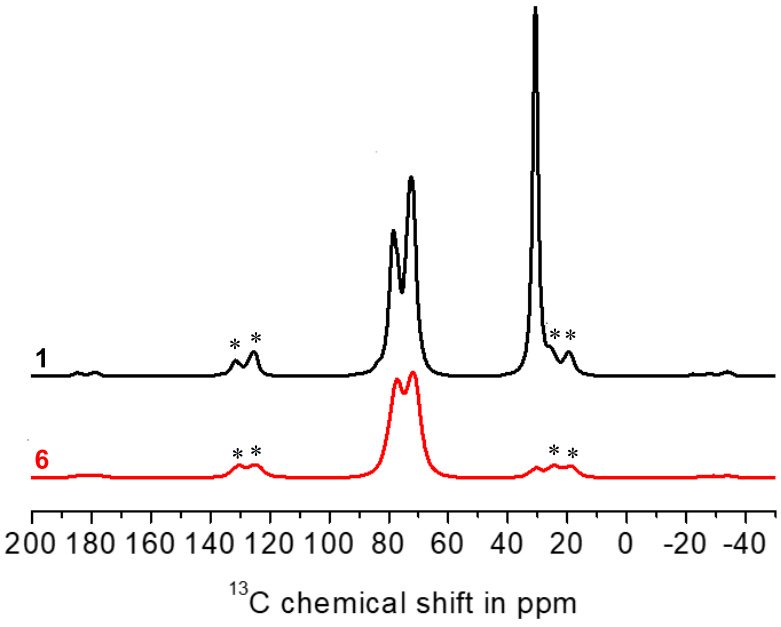

Fig S14. ^{13}C CP MAS NMR spectra of **1** (in black) and polymer **6** (in red), measured at 8 kHz spinning.
Note: Spinning sidebands are marked with asterisks.

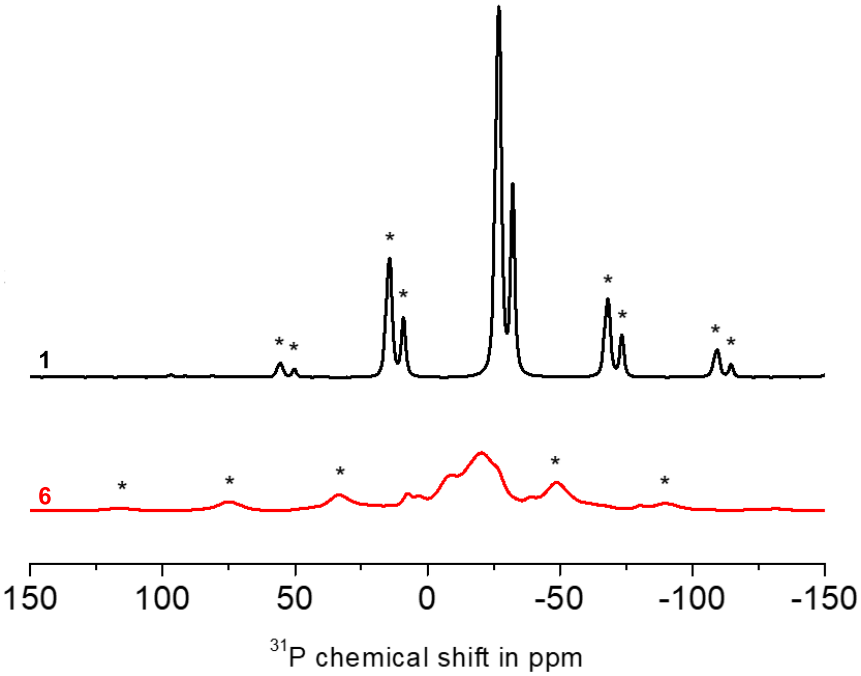

Fig S15. ^{31}P CP MAS NMR spectra of **1** (in black) and polymer **6** (in red), measured at 10 kHz spinning.
Note: Spinning sidebands are marked with asterisks.

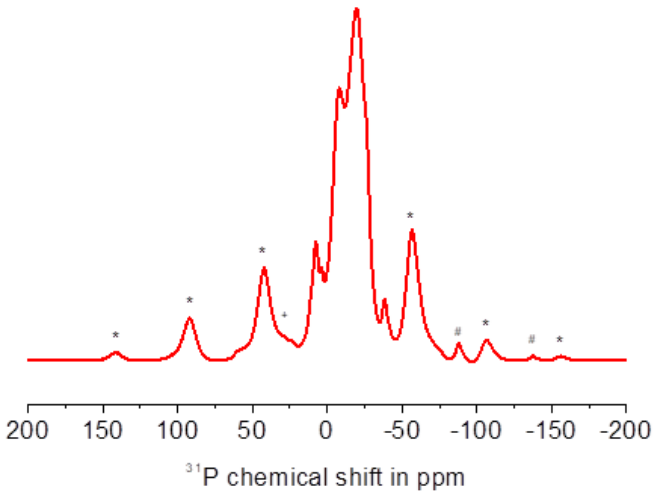

Fig S16. ^{31}P CP MAS NMR spectrum of polymer **6**, measured at 12 kHz spinning.
Note: Spinning sidebands of the broad signals at -8, -20, -26 and -38 ppm are marked with asterisks, plus and hashtags, respectively.

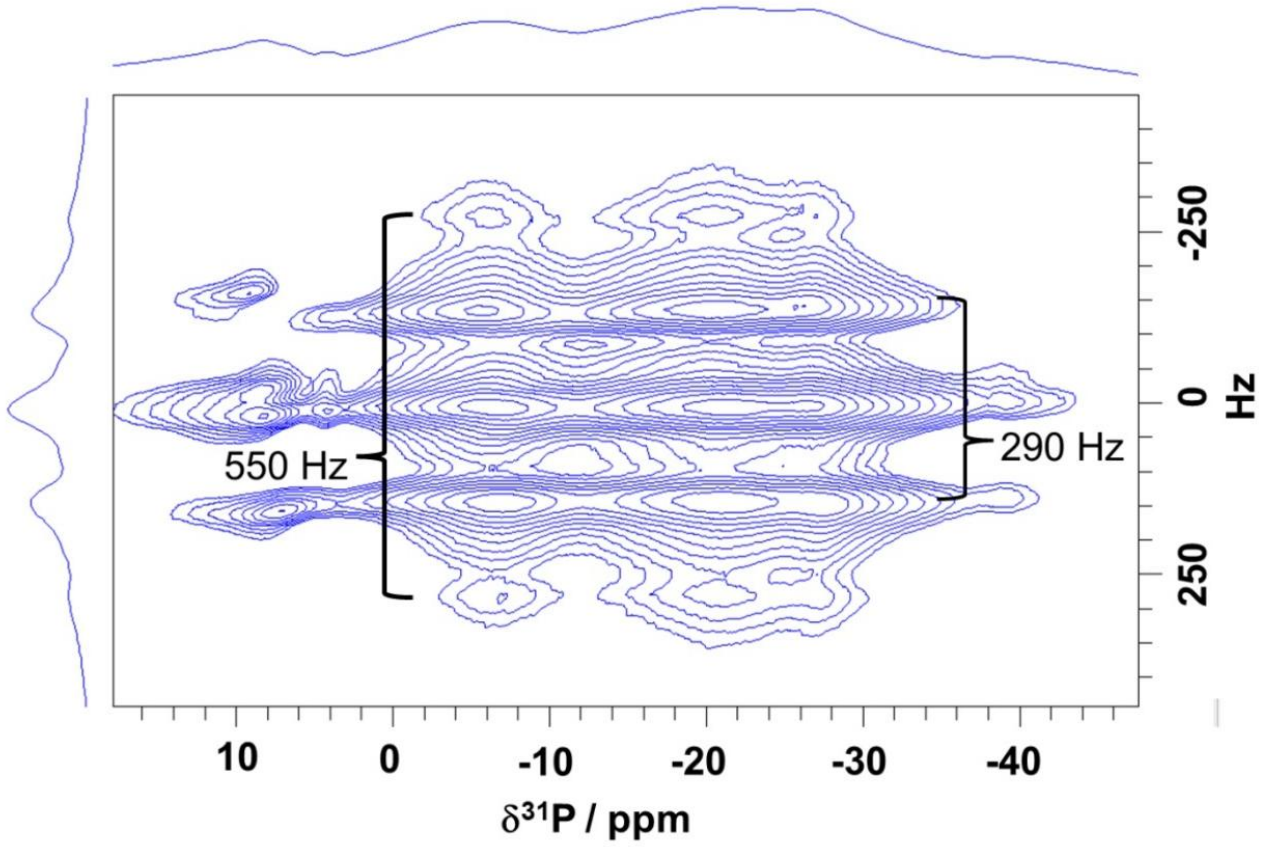

Fig S17. ^{31}P *J*-resolved NMR spectrum of polymer **6**, measured at 12 kHz spinning.

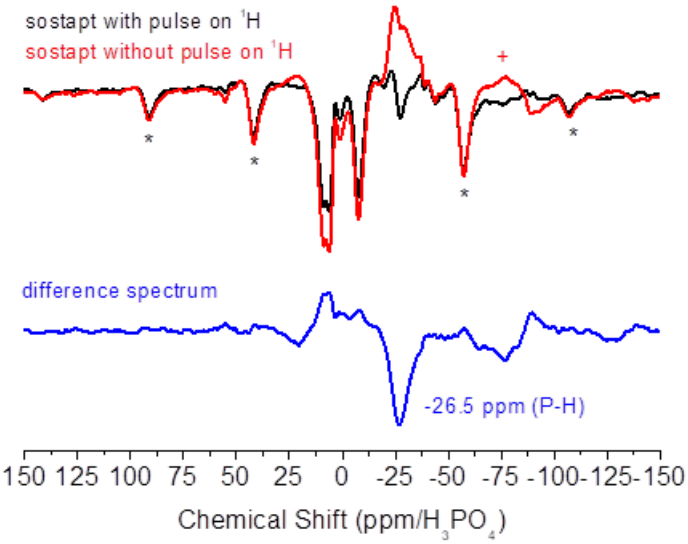

Fig S18. ^{31}P sostapt spectra of polymer **6**, measured at 12 kHz spinning.
Note: The black spectrum was recorded applying pulse power on ^{1}H during inversion of ^{31}P with a 180° pulse. The red spectrum was recorded applying no pulse power on ^{1}H during inversion of ^{31}P with a 180° pulse. This switches all ^{31}P nuclei except those coupled directly to ^{1}H. The blue spectrum shows the difference spectrum indicating the ^{31}P signals of phosphorus directly coupled to ^{1}H as signals with negative amplitude.

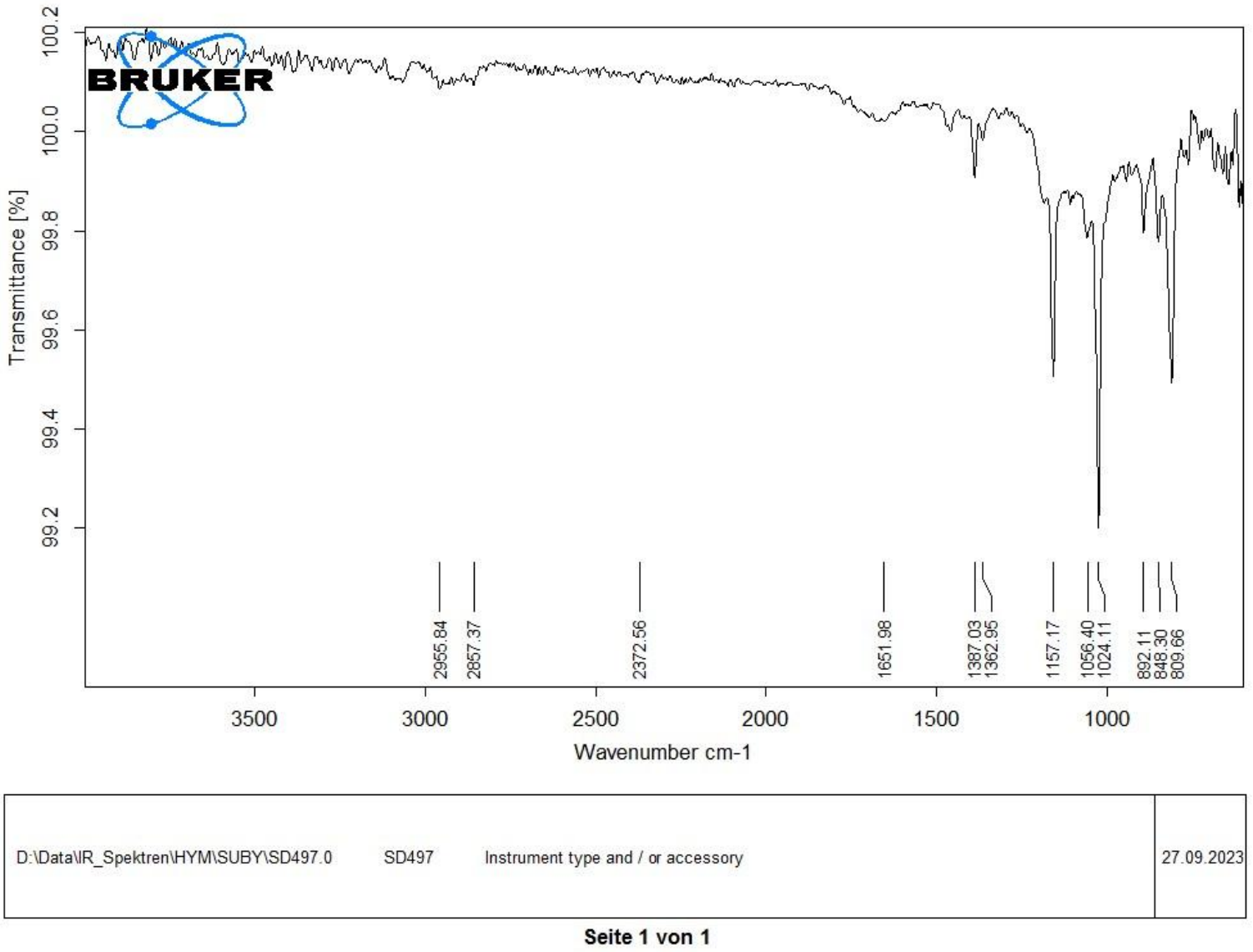

Fig S19. Solid state ATR-IR spectrum of polymer **6**.

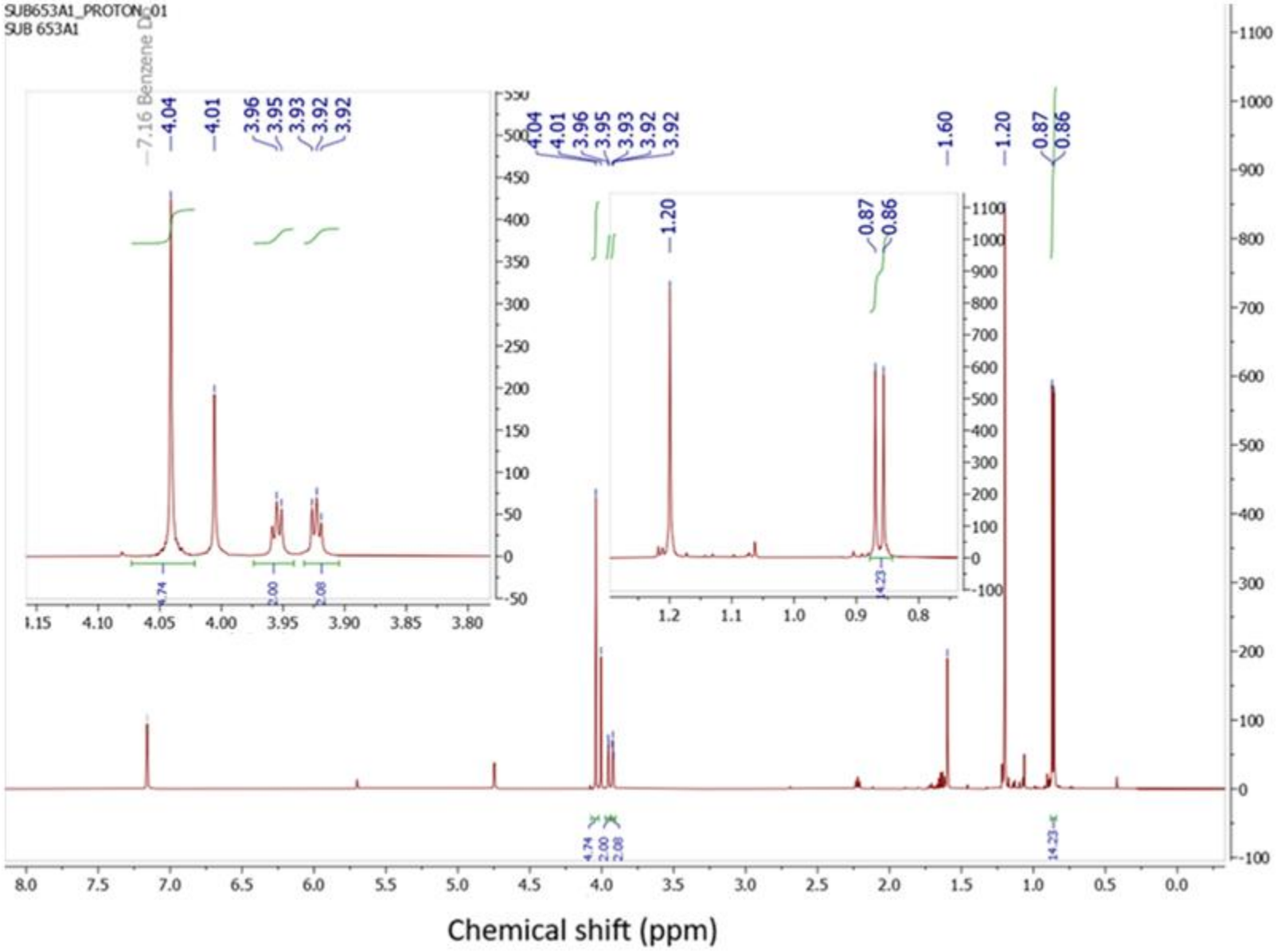

Fig S20. ^{1}H spectroscopic analysis from the crude of polymerization reaction of Fc'(P^{t}Bu$_2$)$_2$.
NOTE: Signals at δ 0.87, 3.92, 3.96 and 4.04 are resulting from Fc^{t}Bu (**8**), whereas signal at δ 1.20 is resulting from ^{t}Bu-^{t}Bu.

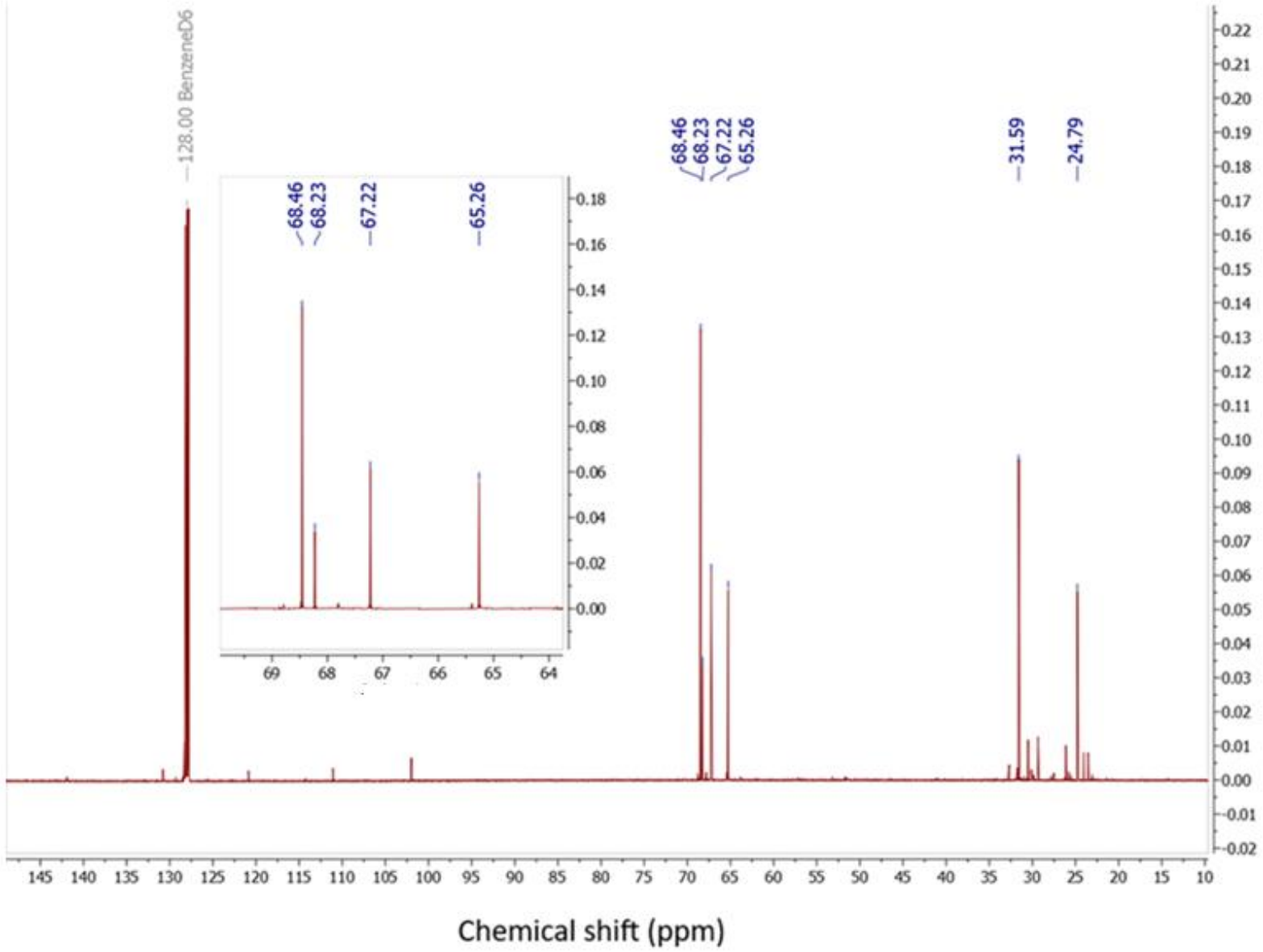

Fig S21. ^{13}C spectroscopic analysis from the crude of polymerization reaction of Fc'(P^tBu_2)$_2$.

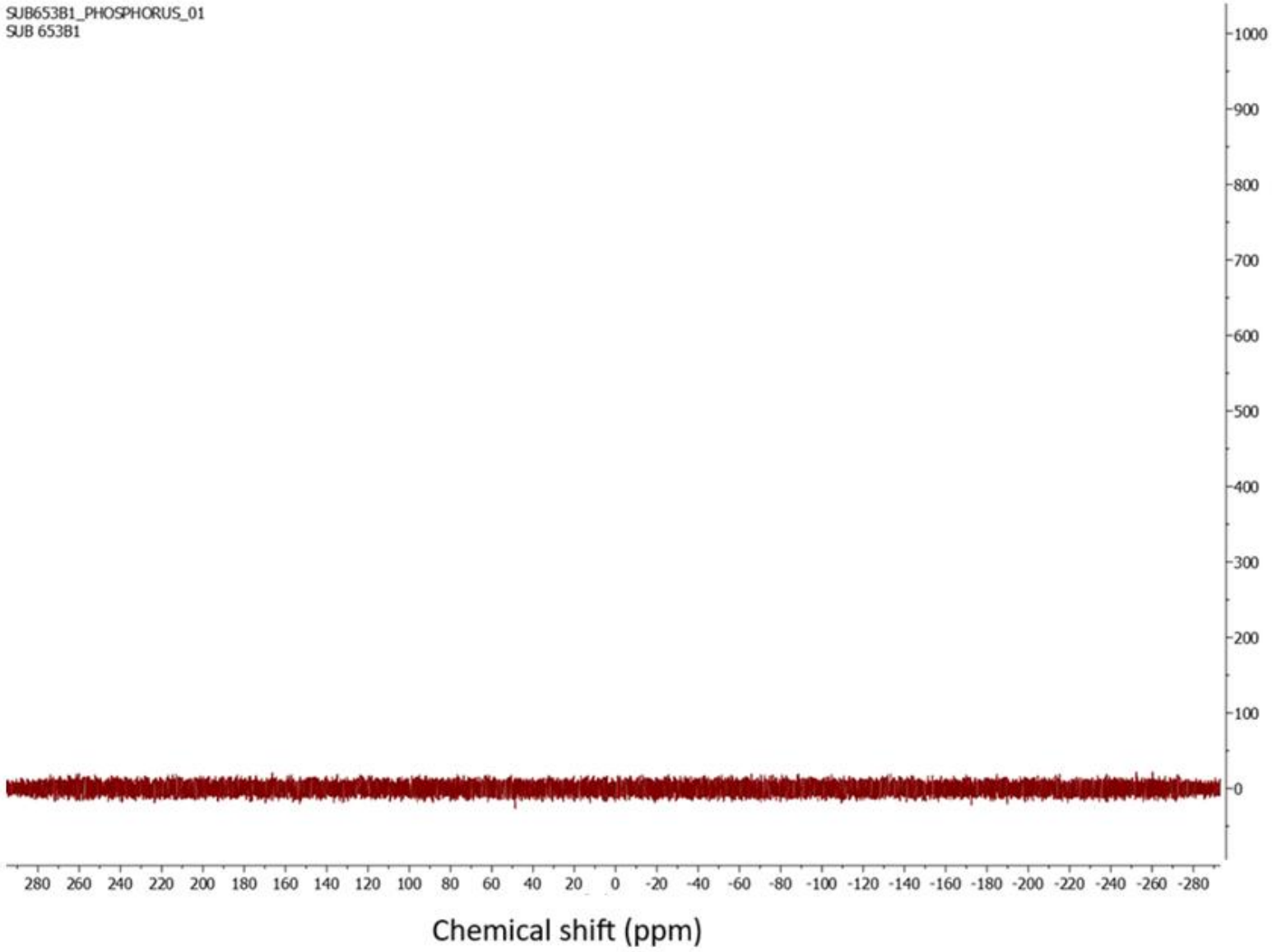

Fig S22. $^{31}P\{^{1}H\}$ spectroscopic analysis from the crude of polymerization reaction of Fc'(P^tBu_2)$_2$.
NOTE: The empty baseline signifies the absence of any soluble P-containing species in the reaction mixture.

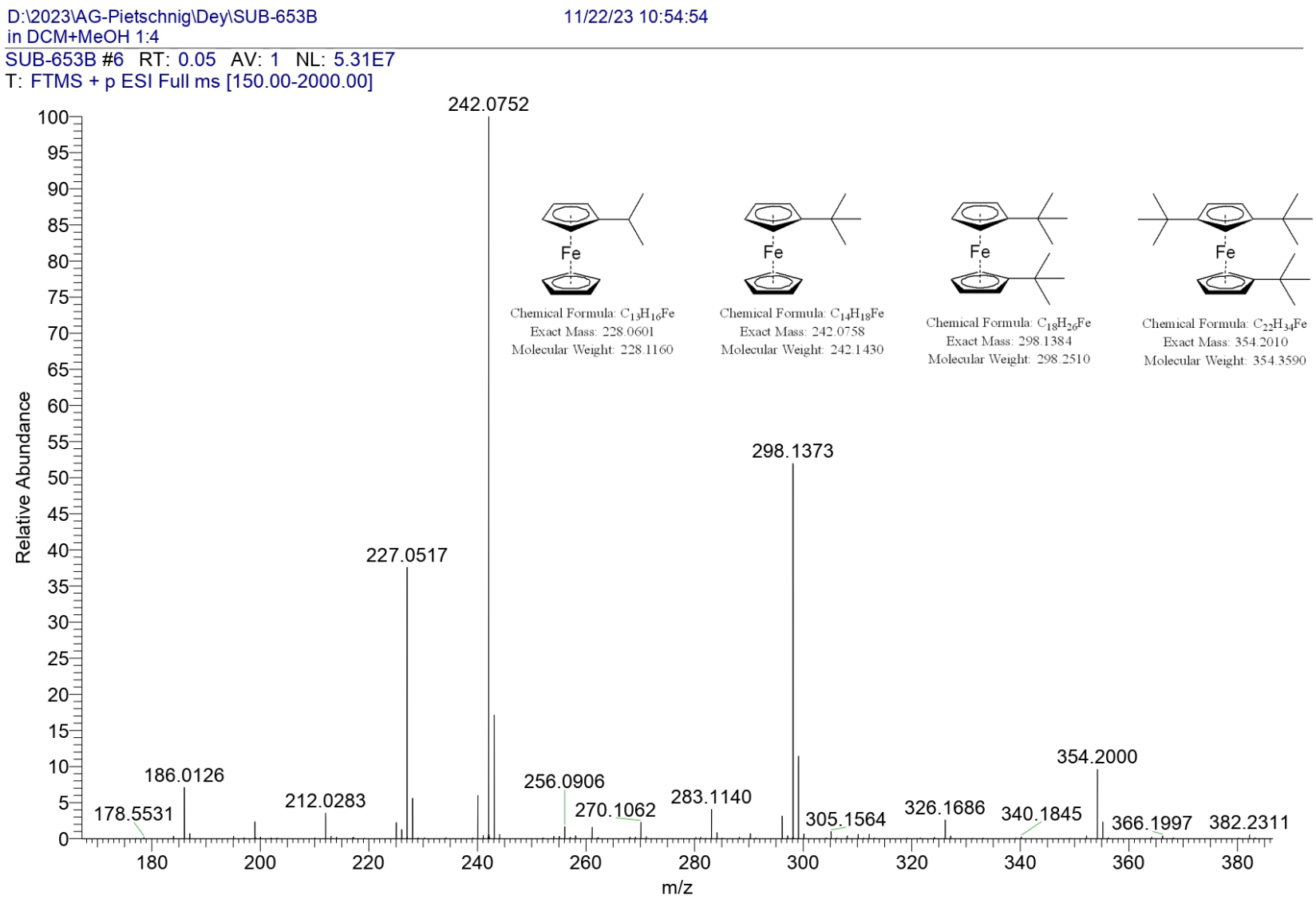

Fig S23. MALDI spectrometric analysis from soluble fraction from polymerization reaction of Fc'($PtBu_2$)$_2$.

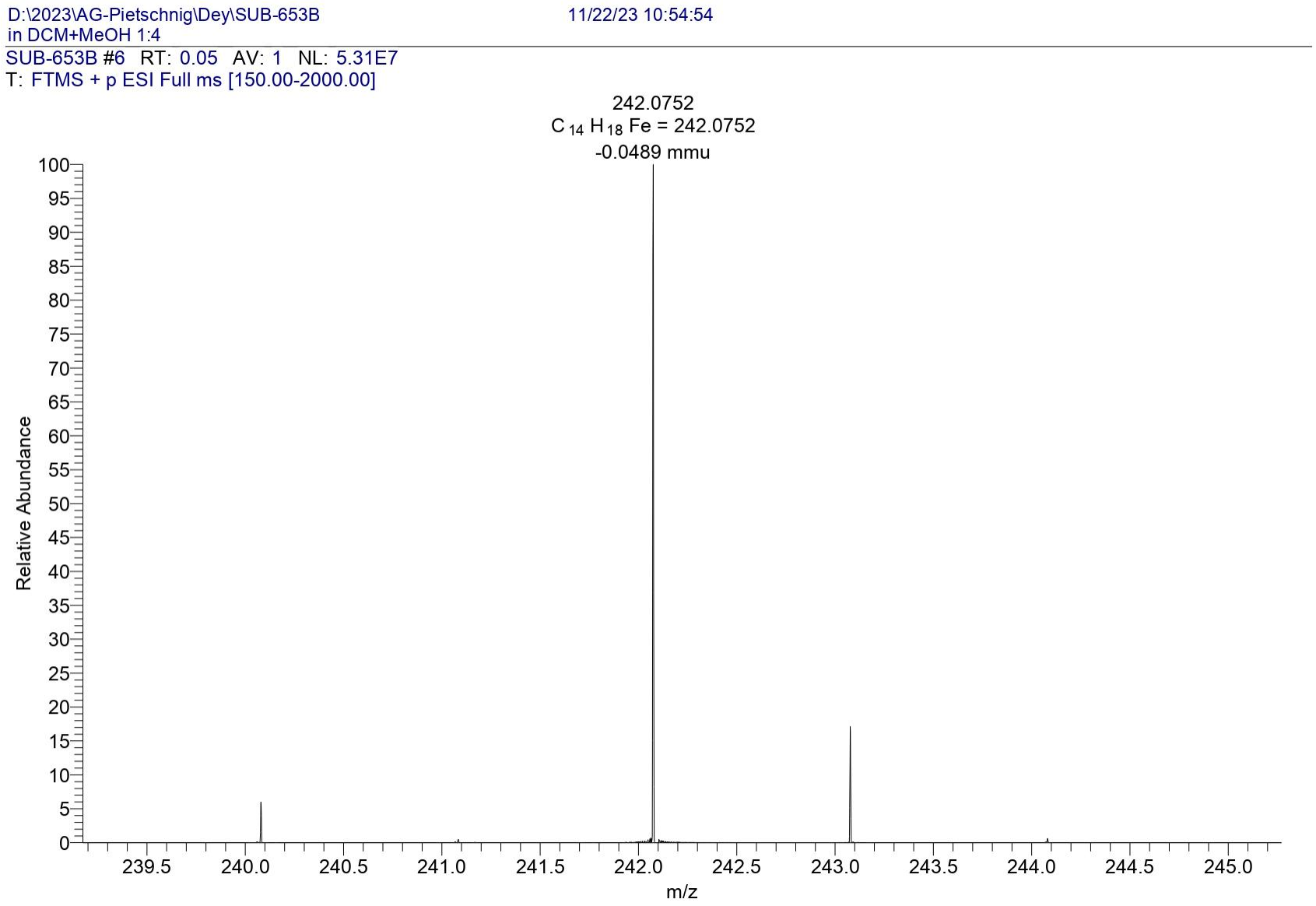

Fig S24. MALDI (HRMS) spectrometric analysis for Fc(*t*Bu)

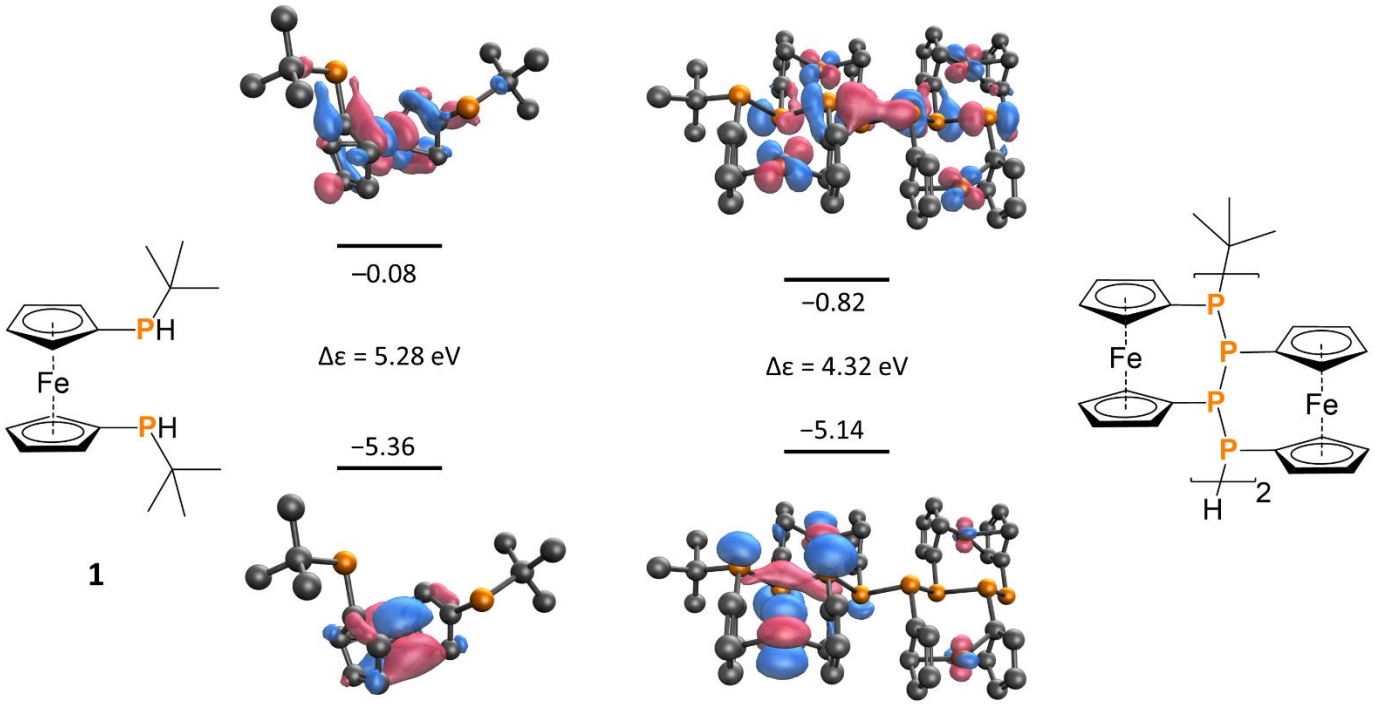

Fig S25. Kohn–Sham frontier molecular orbitals and corresponding energy levels (in eV) for compound **1** and the oligomeric model system
(computed at B3LYP/6-31G*//ωB97X-D/6-311+G** level of theory)

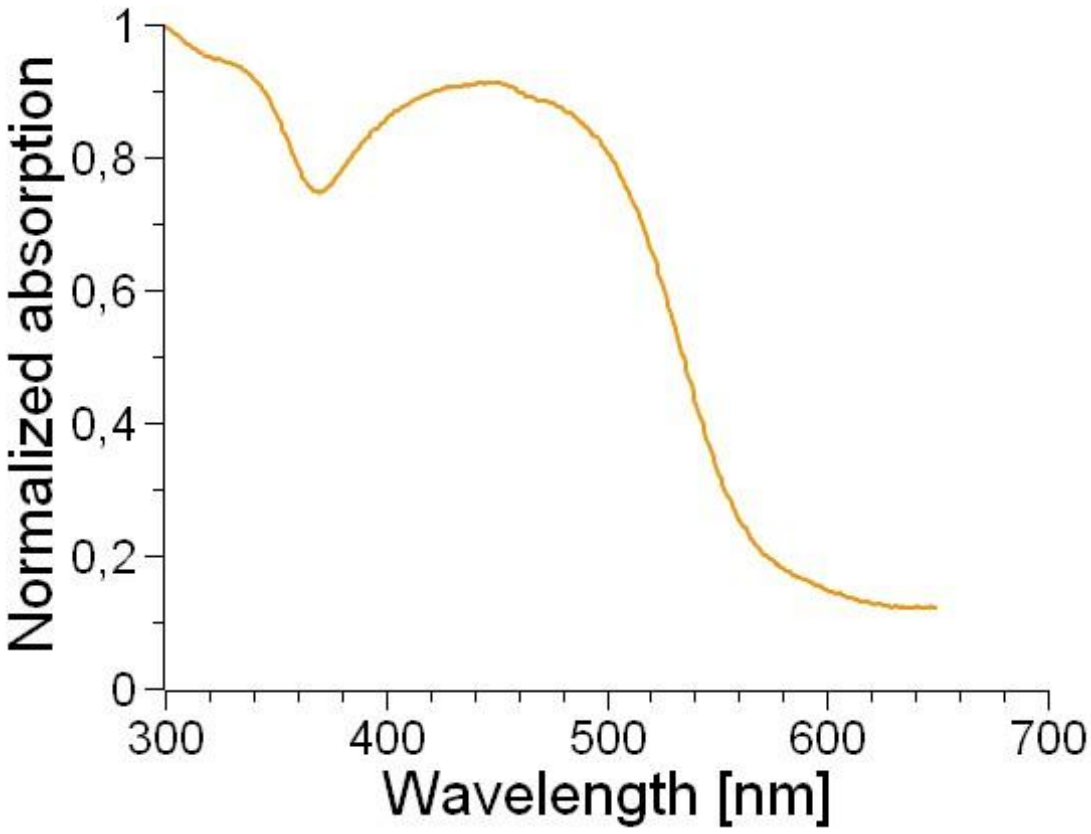

Fig S26. Solid state UV-Vis spectra of compound **1**.

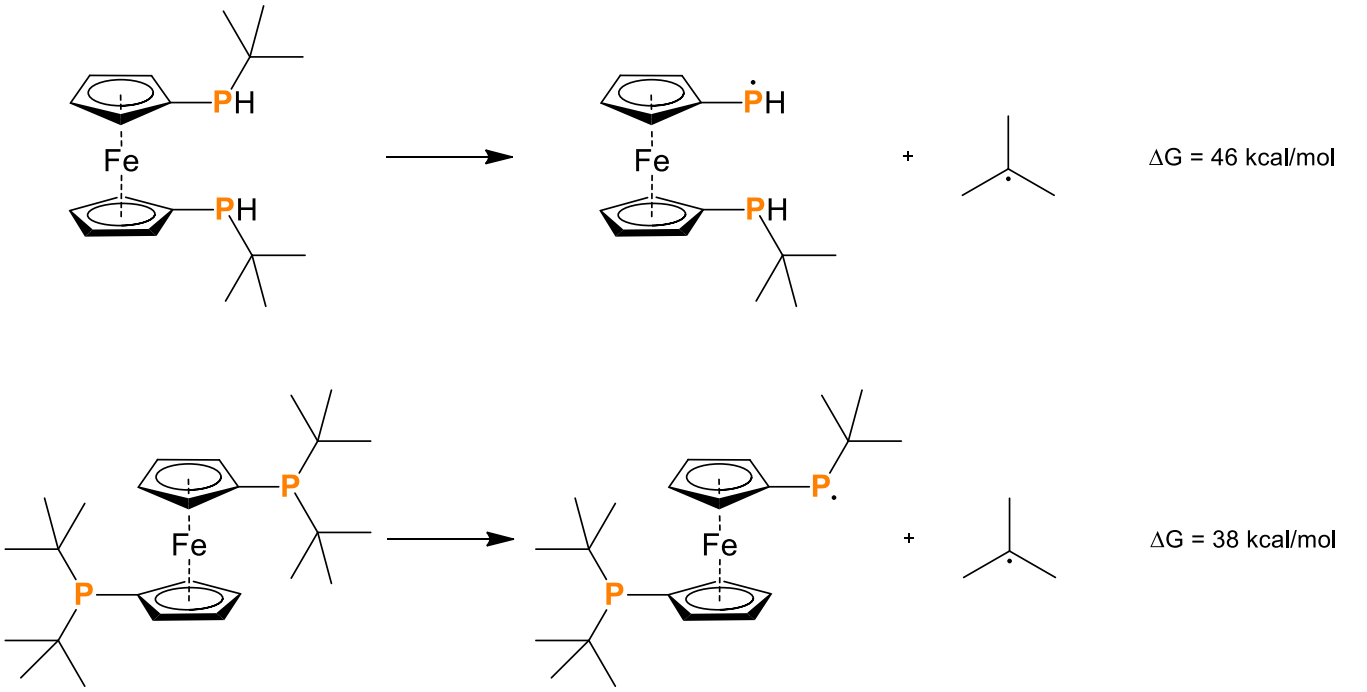

Scheme S1. The cleavage of the P–C(tBu) bond in cases of **1** and **8**.

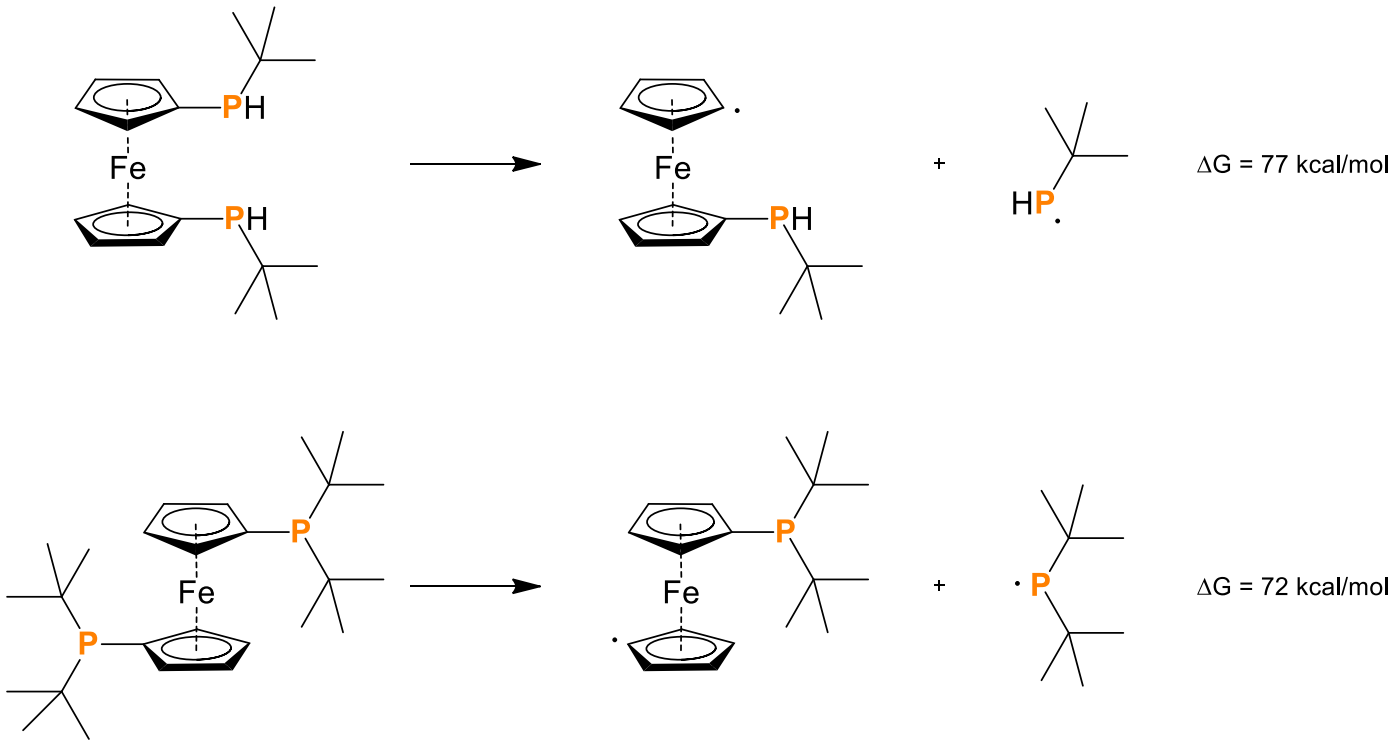

Scheme S2. The cleavage of the Fc–P bond in cases of **1** and **8**.

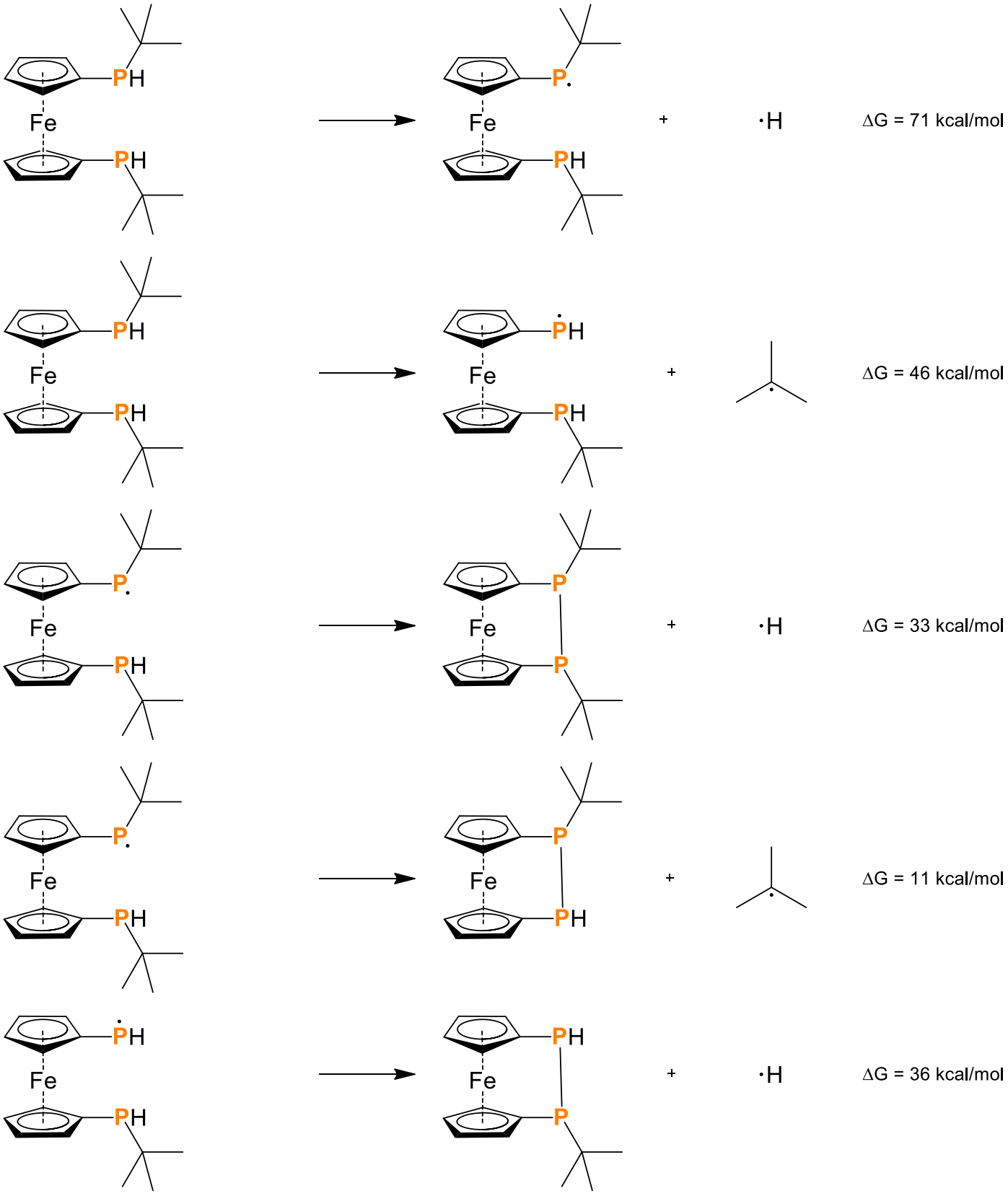
Fe
PH
P
·H
ΔG = 71 kcal/mol
ΔG = 46 kcal/mol
ΔG = 33 kcal/mol
ΔG = 11 kcal/mol
ΔG = 36 kcal/mol

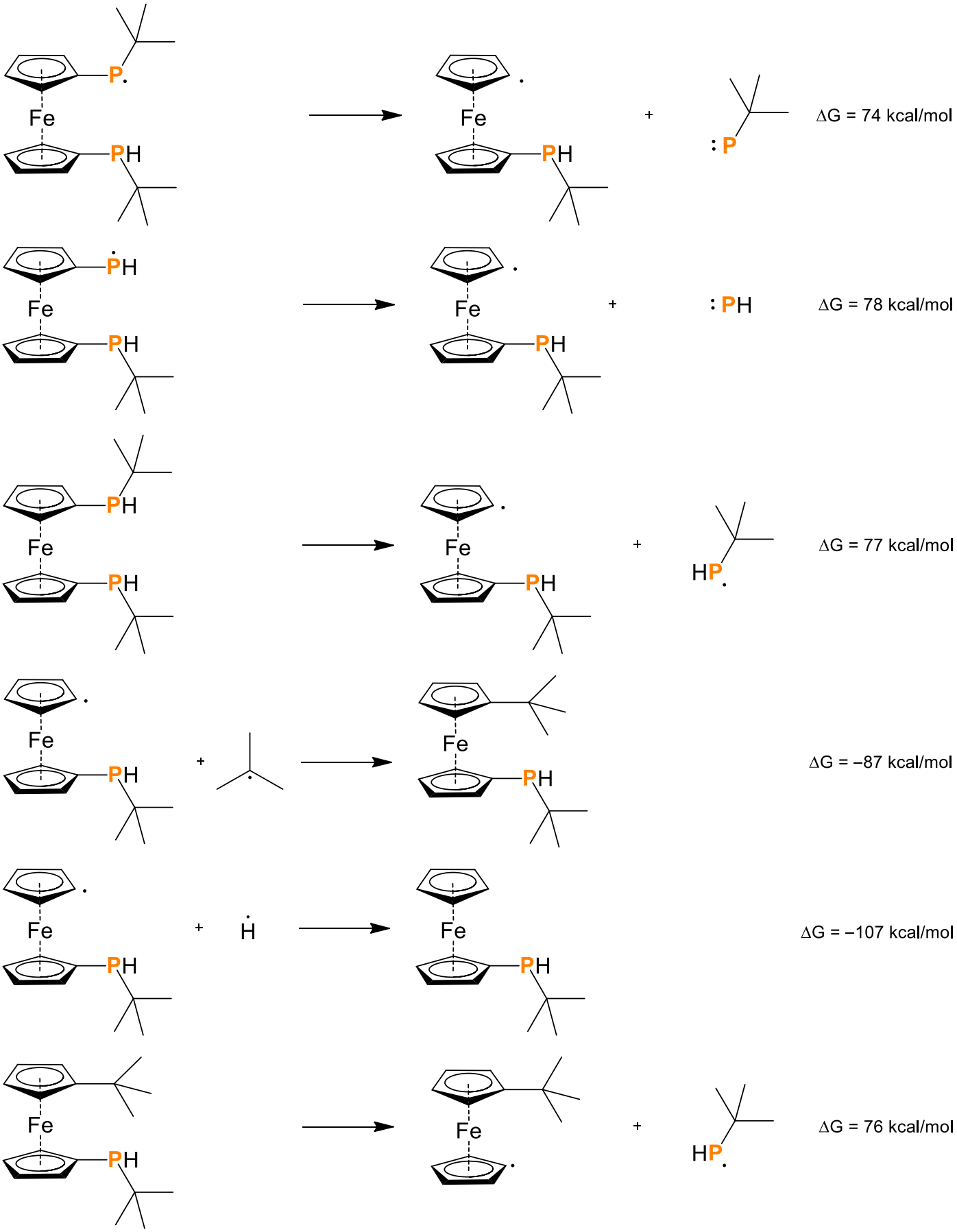
Fe
PH
ΔG = 74 kcal/mol
ΔG = 78 kcal/mol
ΔG = 77 kcal/mol
ΔG = –87 kcal/mol
ΔG = –107 kcal/mol
ΔG = 76 kcal/mol

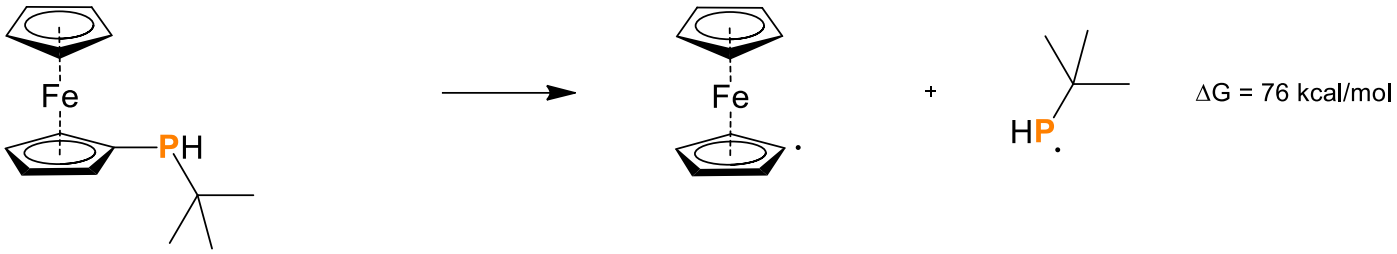
Fe
PH
Fe
HP
ΔG = 76 kcal/mol

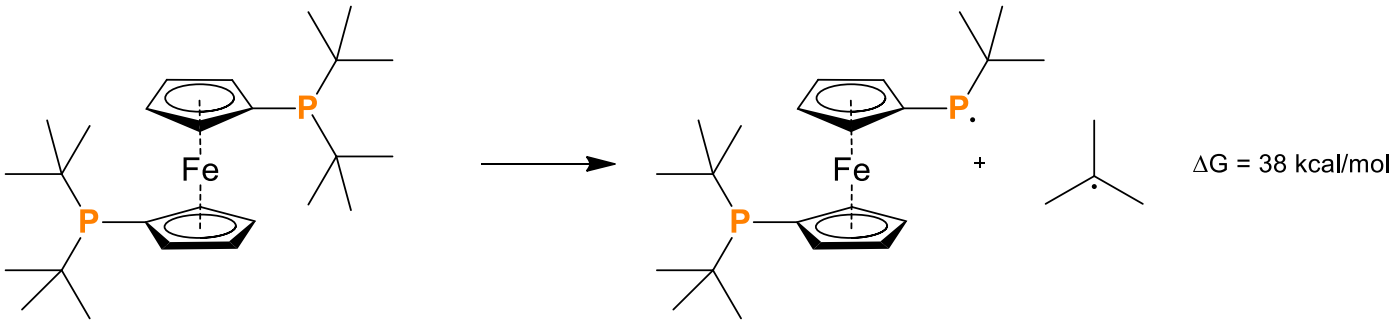
P
Fe
P
P
Fe
P
ΔG = 38 kcal/mol

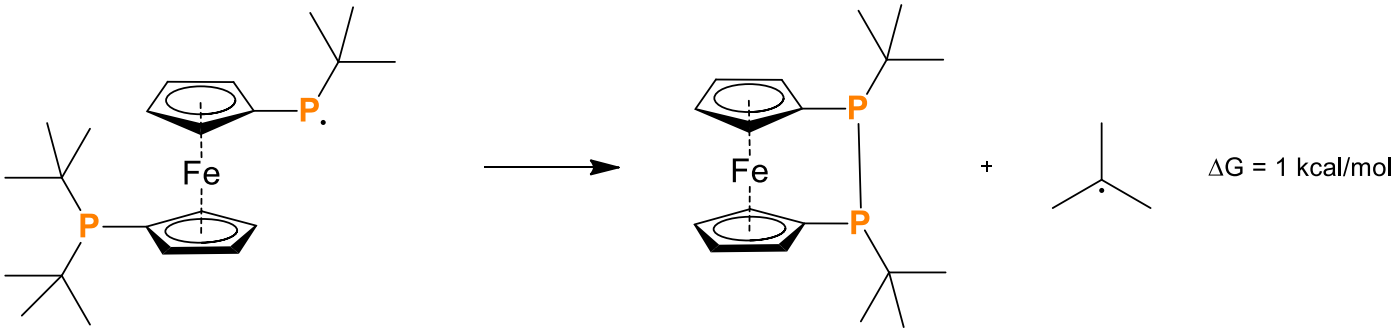
P
Fe
P
P
Fe
P
ΔG = 1 kcal/mol

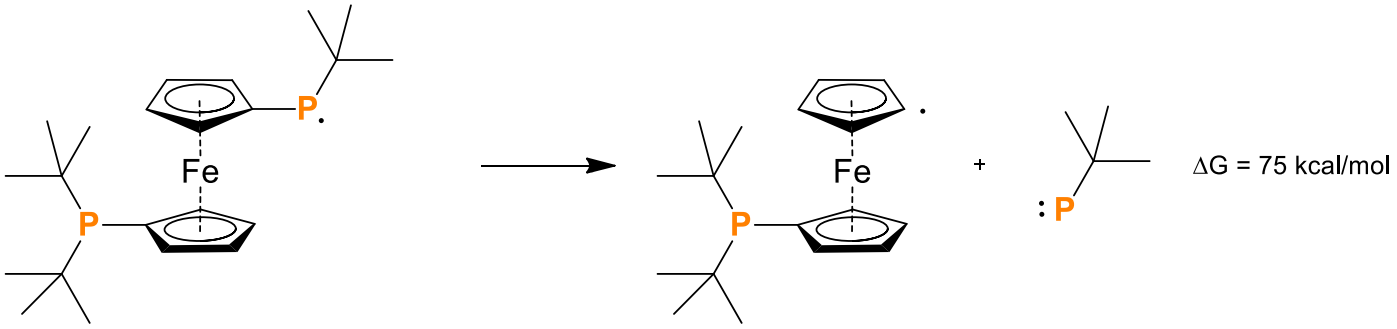
P
Fe
P
Fe
P
: P
ΔG = 75 kcal/mol

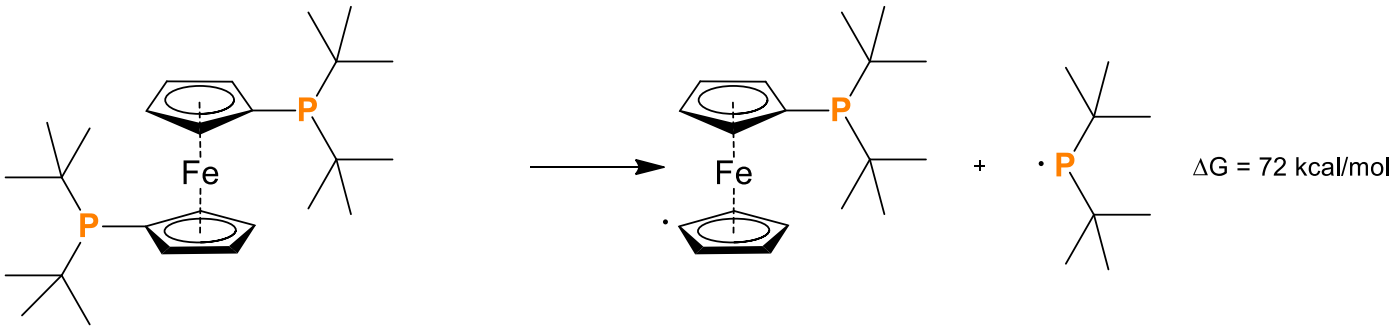
P
Fe
P
P
Fe
P
ΔG = 72 kcal/mol

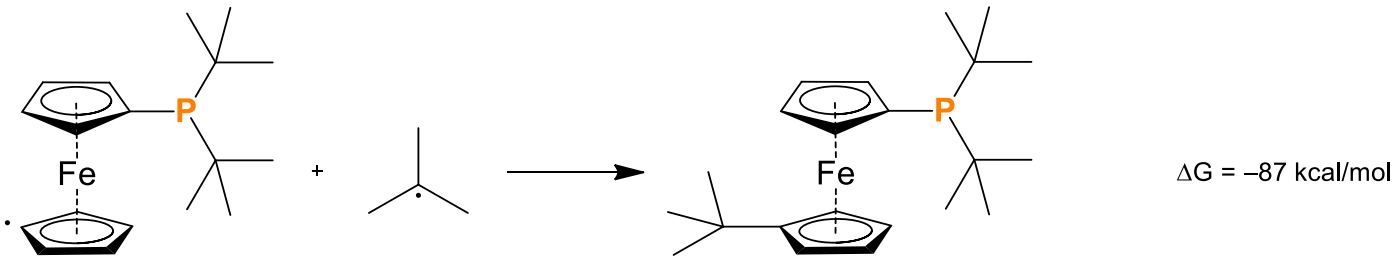
P
Fe
P
Fe
ΔG = –87 kcal/mol

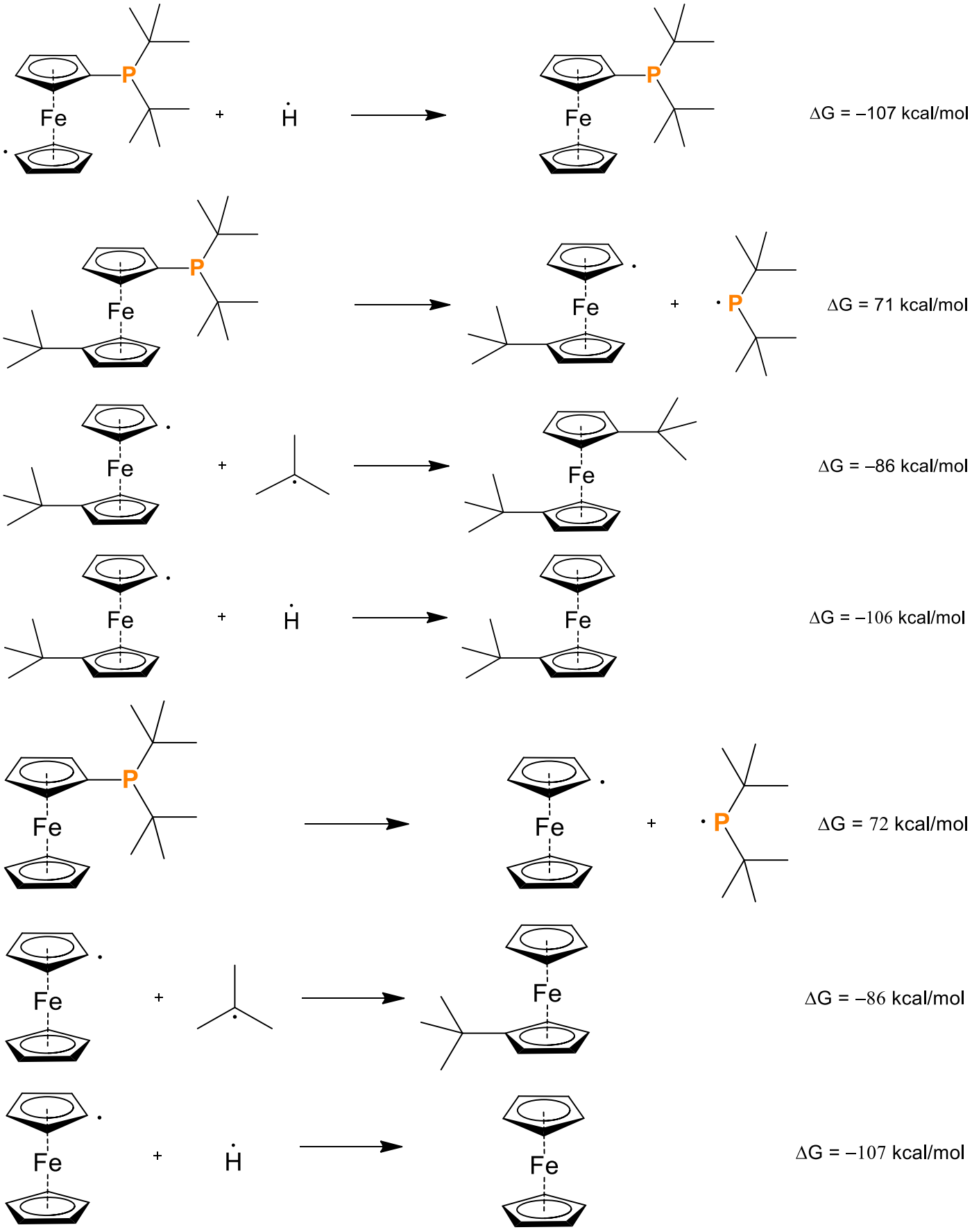

Scheme S3. The investigated alternative pathways.

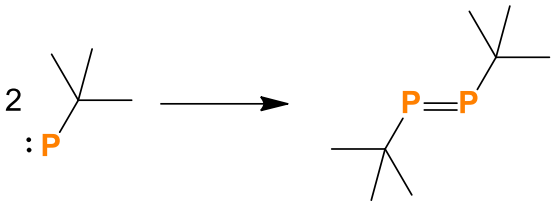

ΔG = –64 kcal/mol

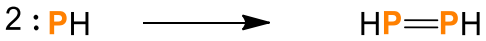

ΔG = –66 kcal/mol

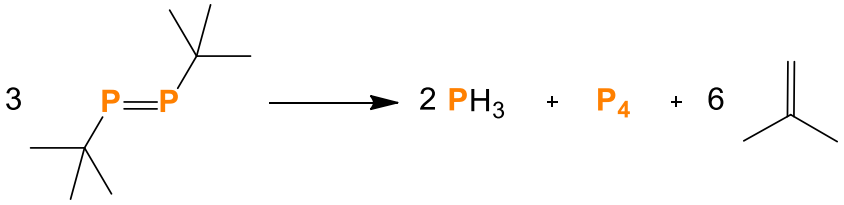

ΔG = –1 kcal/mol

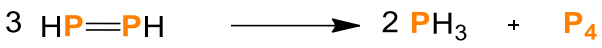

ΔG = –59 kcal/mol

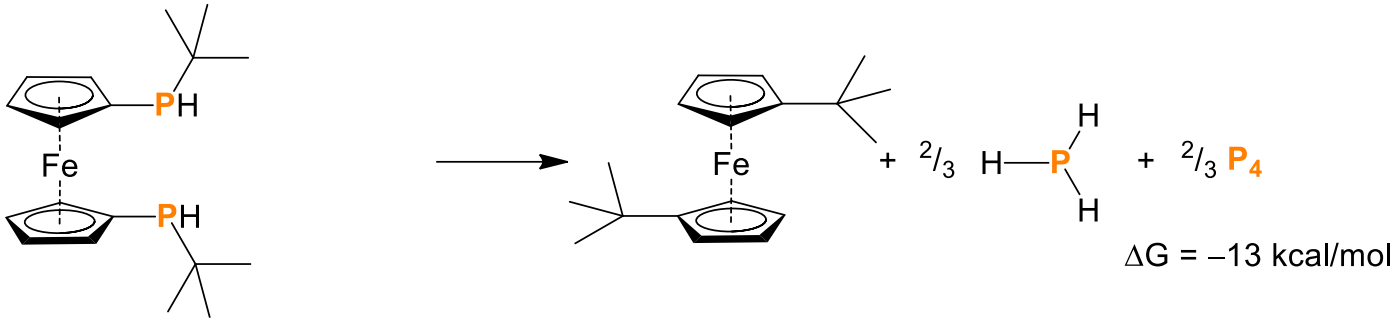

ΔG = –13 kcal/mol

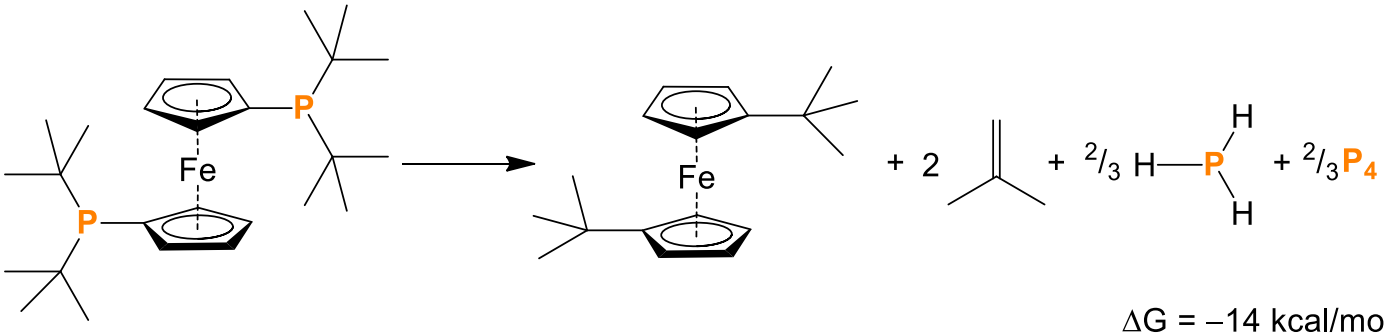

ΔG = –14 kcal/mol

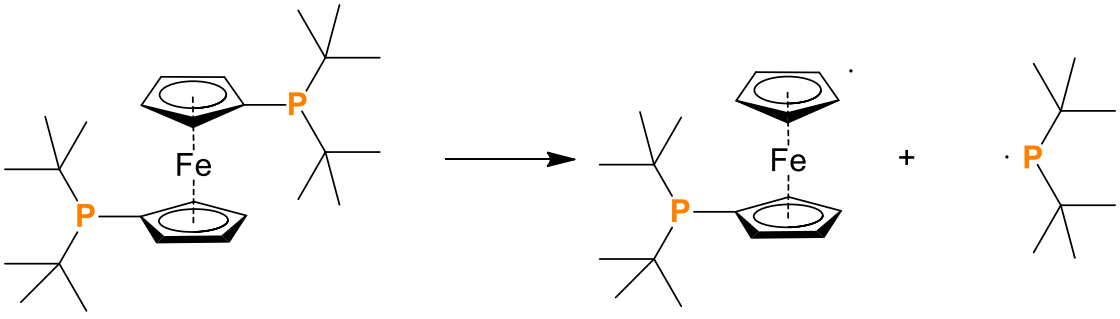

ΔG = 72 kcal/mol

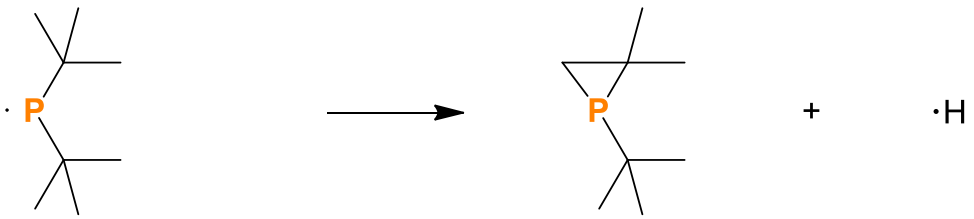

ΔG = 44 kcal/mol

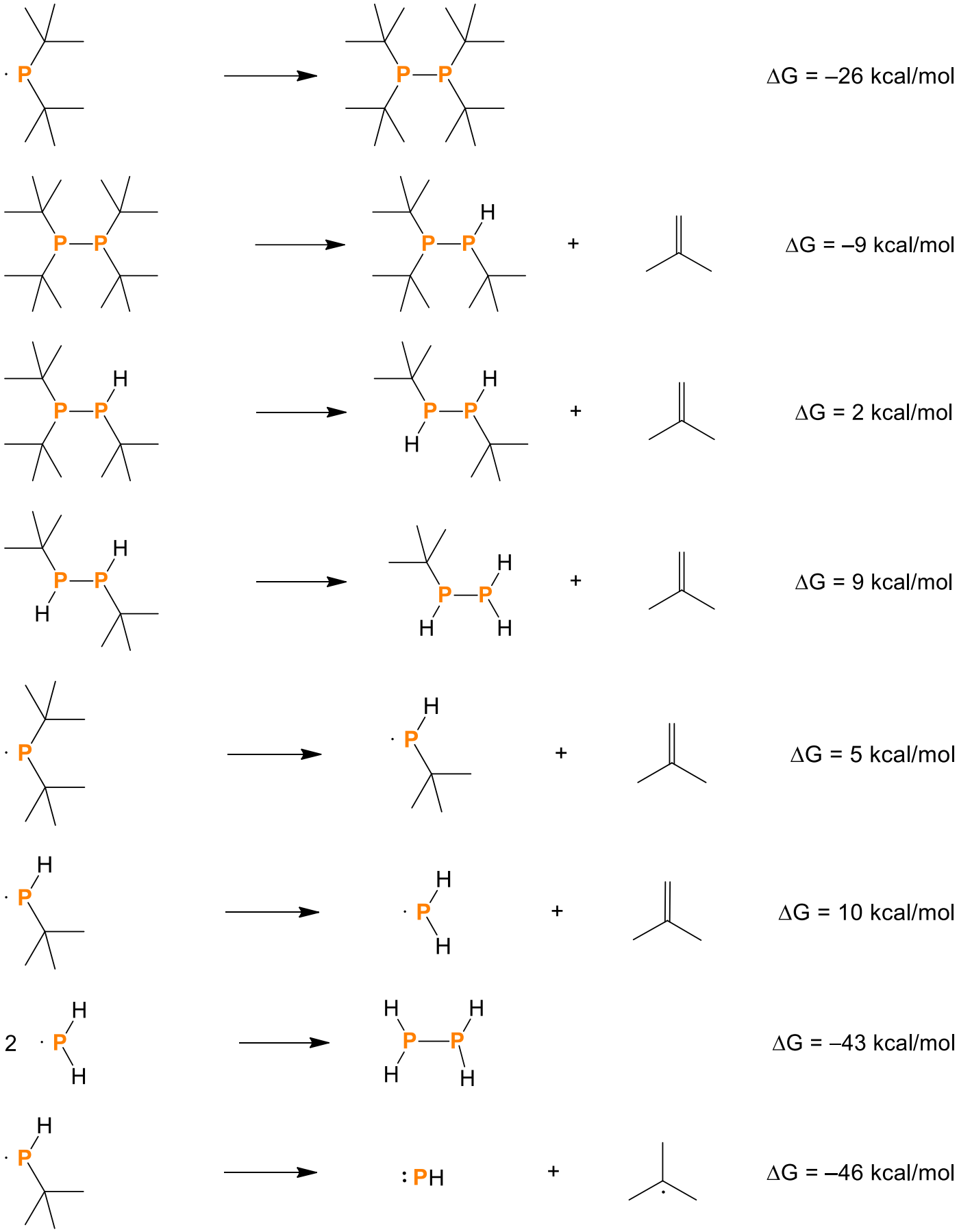
ΔG = –26 kcal/mol
ΔG = –9 kcal/mol
ΔG = 2 kcal/mol
ΔG = 9 kcal/mol
ΔG = 5 kcal/mol
ΔG = 10 kcal/mol
ΔG = –43 kcal/mol
ΔG = –46 kcal/mol

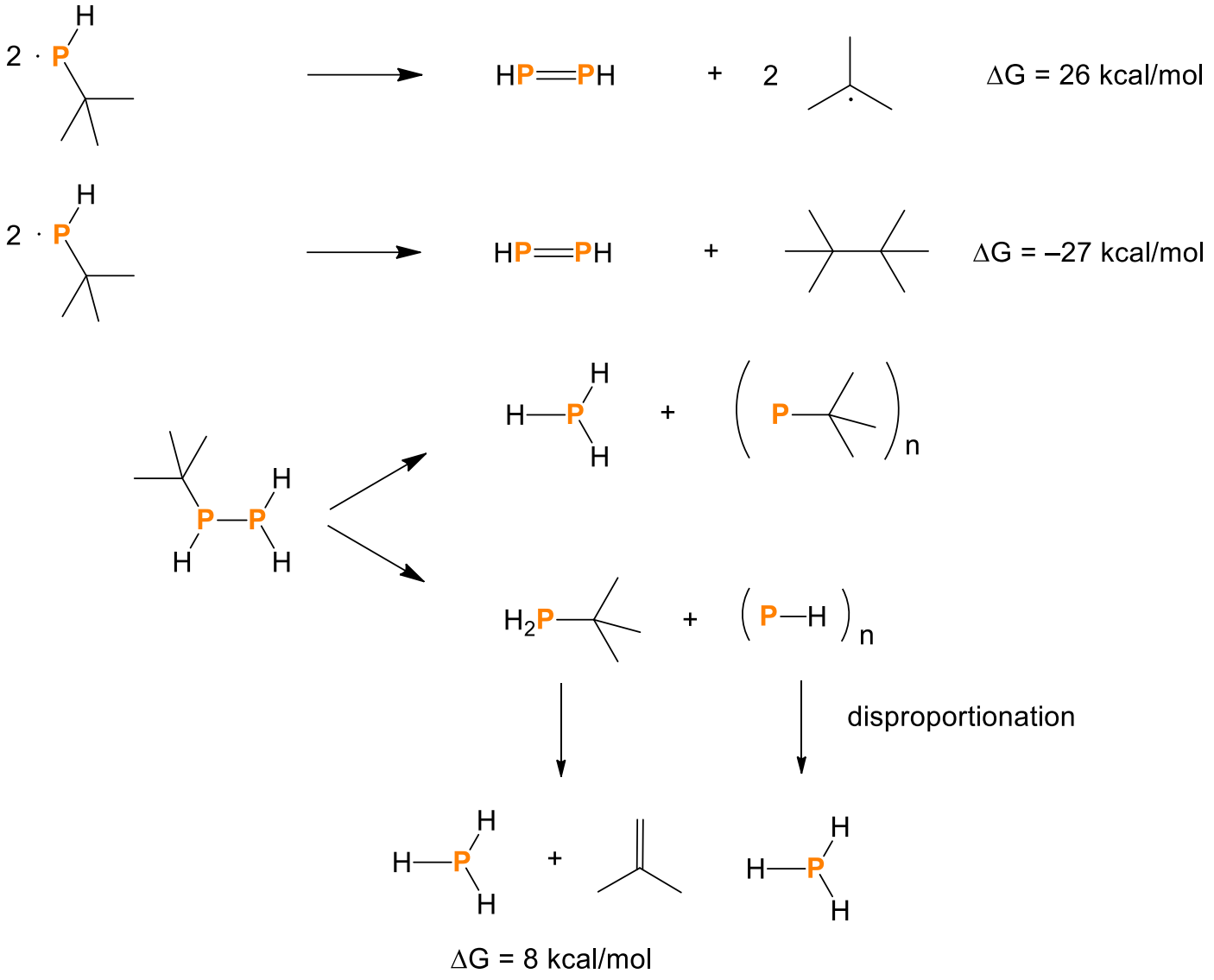

Scheme S4. The considered reaction paths result in volatile phosphorus-containing products.

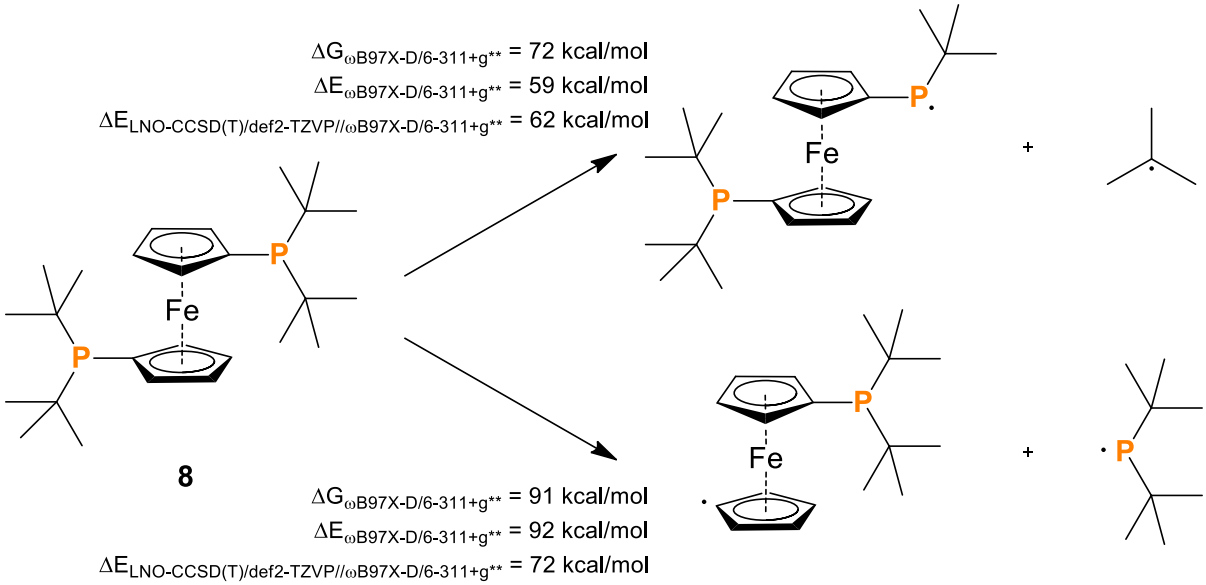

Scheme S5. Thermodynamic profile of the thermal decomposition pathways of Fc′($PtBu_2$)$_2$ (computed at the ωB97X-D/6-311+G** level of theory, with LNO-CCSD(T)/def2-TZVP single-point energies evaluated on ωB97X-D/6-311+G** optimized geometries)

References

[1] S. Dey, B. Szathmari, R. Franz, C. Bruhn, Z. Kelemen, R. Pietschnig, *Chem. Eur. J.* **2024**, *30*, e202400194.